

## REPORT DOCUMENTATION PAGE

AFRL-SR-BL-TR-99-

Public reporting burden for this collection of information is estimated to average 1 hour per response, including the time for reviewing instructions, searching existing data sources, gathering the data, reviewing the collection of information, Send comments regarding this burden estimate or any other aspect of this collection of information, including suggestions for reducing the burden, to Washington Headquarters Services, Directorate for Information Operations and Reports, 1215 Jefferson Davis Highway, Suite 1204, Arlington, VA 22202-4302, and to the Office of Management and Budget, Paperwork Project, Washington, DC 20503.

1 reviewing  
information

1. AGENCY USE ONLY (Leave blank)		2. REPORT DATE November 1999	3. REPORT TYPE AND DATES COVERED FINAL TECHNICAL REPORT 1 May 97 - 31 Dec 97
4. TITLE AND SUBTITLE MICROSCALE PLASTICITY AND FRACTURE TOUGHNESS OF Ti3SiC2 AT AMBIENT AND HIGH TEMPERATURES			5. FUNDING NUMBERS F49620-97-1-0298  2306/BS 61102F
6. AUTHOR(S) M. W. BARSOUM			
7. PERFORMING ORGANIZATION NAME(S) AND ADDRESS(ES) DREXEL UNIVERSITY DEPARTMENT OF MATERIALS ENGINEERING PHILADELPHIA PA 19104			8. PERFORMING ORGANIZATION REPORT NUMBER
9. SPONSORING/MONITORING AGENCY NAME(S) AND ADDRESS(ES) AIR FORCE OFFICE OF SCIENTIFIC RESEARCH 110 DUNCAN AVENUE SUITE B115 BOLLING AFB DC 20332-8050			10. SPONSORING/MONITORING AGENCY REPORT NUMBER
11. SUPPLEMENTARY NOTES  <div style="text-align: right; font-size: 2em; font-weight: bold;">19991227 039</div>			
12a. DISTRIBUTION AVAILABILITY STATEMENT APPROVED FOR PUBLIC RELEASE, DISTRIBUTION IS UNLIMITED			12b. DISTRIBUTION CODE
13. ABSTRACT (Maximum 200 words) The goal of this work was to develop a science-based understanding of the structure property relationships in Ti3SiC2. Late in 1995 we synthesized for the first time dense, bulk single phase samples of Ti3SiC2. Preliminary characterization has shown it to be a ternary compound with a unique set of properties, machinability similar to that of graphite, excellent oxidation resistance, relatively low density 4.5 gm/cm3 and non-susceptibility to thermal shock. A brittle-to-ductile transition occurs at 1200 °C, and at 1300 °C the material is plastic with very respectable yield points (100 and 500 MPa in flexure and compression, respectively). This combination of properties renders Ti3SiC2 an attractive candidate for a variety of high temperature structural applications of interest to the Air Force and creates the immediate need for a detailed characterization study to understand the physical origin of these properties. The evolution of deformation-microfracture damage below Hertzian contacts in a coarse-grained Ti3SiC2 was studied. The Hertzian indentation stress-strain response deviates strongly from linearity beyond a well-defined maximum, with pronounced strain-softening, indicating exceptional deformability in this otherwise (elastically) stiff ceramic. Surface and subsurface ceramographic observations reveal extensive quasi-plastic microdamage zones at the contact sites. The ternary carbide, Ti3SiC2, fabricated by a reactive hot press route was investigated by transmission electron microscopy, TEM. The material consists mainly of large elongated grains with planar boundaries and is characterized by a low defect density. Dislocations are observed in the grains and at grain boundaries. Perfect dislocations with $b = 1/3 \cdot 1120$ lying in (0001) basal planes are present.			
14. SUBJECT TERMS			15. NUMBER OF PAGES
			16. PRICE CODE
17. SECURITY CLASSIFICATION OF REPORT  U	18. SECURITY CLASSIFICATION OF THIS PAGE  U	19. SECURITY CLASSIFICATION OF ABSTRACT  U	20. LIMITATION OF ABSTRACT

DTIC QUALITY INSPECTED 2

Standard Form 298 (Rev. 2-89) (EG)  
Prescribed by ANSI Std. Z39.18  
Designed using Perform Pro, WWS/DIOR, Oct 84

1 7 NOV 1999

Final Report

On

**MICROSCALE PLASTICITY AND FRACTURE TOUGHNESS  
OF  $\text{Ti}_3\text{SiC}_2$   
AT AMBIENT AND HIGH TEMPERATURES**

By

M. W. Barsoum

Department of Materials Engineering  
Drexel University, Philadelphia PA 19104

**Proposal Number**

**F49620-97-1-0298**

**Contract Monitor**

**Dr. Alexander Pechenik  
U.S. Air Force, AFOSR-NC  
Bolling AFB,  
110 Duncan Ave., Wash. DC  
703 696 7236**

## I. INTRODUCTION

*Abstract*

The goal of the ~~proposed~~ work was to develop a science-based understanding of the structure-property relationships in  $\text{Ti}_3\text{SiC}_2$ . Late in 1995 we synthesized for the first time dense, bulk single phase samples of  $\text{Ti}_3\text{SiC}_2$ . Preliminary characterization has shown it to be a ternary compound with a unique set of properties; machinability similar to that of graphite, excellent oxidation resistance, relatively low density ( $4.5 \text{ gm/cm}^3$ ) and non-susceptibility to thermal shock. A brittle-to-ductile transition occurs at  $1200^\circ\text{C}$ , and at  $1300^\circ\text{C}$  the material is plastic with very respectable yield points (100 and 500 MPa in flexure and compression, respectively). This combination of properties renders  $\text{Ti}_3\text{SiC}_2$  an attractive candidate for a variety of high temperature structural applications of interest to the Air Force and creates the immediate need for a detailed characterization study to understand the physical origin of these properties.

In May 1997 we were awarded an 7 month grant from AFOSR to continue working on  $\text{Ti}_3\text{SiC}_2$ . Using this funding we published 5 refereed publications [1-5]. The main results are summarized below and the papers are attached to this report.

- i) In this work we delineated the reaction path and microstructure evolution during the reactive hot isostatic processing of  $\text{Ti}_3\text{SiC}_2$ , starting with Ti, SiC and graphite powders [1]. A series of interrupted hot isostatic press runs are carried out as a function of temperature ( $1200\text{-}1600^\circ\text{C}$ ) and time (0-24 hours). Based on X-ray diffraction and scanning electron microscopy, at  $1200^\circ\text{C}$  the intermediate phases are  $\text{TiC}_x$  and  $\text{Ti}_5\text{Si}_3\text{C}_x$ . Fully dense, essentially single phase, samples are fabricated in the  $1450\text{-}1700^\circ\text{C}$  temperature range. The time-temperature processing envelope for fabricating microstructures with small ( $\approx 3\text{-}5$ ), large ( $\approx 200 \mu\text{m}$ ) and duplex grains, in which large ( $100\text{-}200 \mu\text{m}$ ) grains of  $\text{Ti}_3\text{SiC}_2$  are embedded in a much finer matrix, is delineated. The microstructure evolution is to a large degree determined by: i) the presence of unreacted phases, mainly  $\text{TiC}_x$ , that inhibits grain growth, and ii) a large anisotropy in growth rates along the c and a -directions; at  $1450^\circ\text{C}$ , growth normal to the basal planes is roughly an order of magnitude smaller than that parallel to these planes; at  $1600^\circ\text{C}$  the ratio is 4, and; iii) impingement of the grains.  $\text{Ti}_3\text{SiC}_2$  is thermally stable under vacuum and Ar atmosphere at temperatures as high as  $1600^\circ\text{C}$  for up to 24 hours. This work was published in the Journal of the American Ceramic Soc. in Oct. 1999. A reprint is attached to the end of this report.
- ii) In this work [2] we report on the mechanical behavior of  $\text{Ti}_3\text{SiC}_2$ , described in the aforementioned paper[1]. In particular, we have evaluated the mechanical response of fine-grained  $\text{Ti}_3\text{SiC}_2$  ( $3\text{-}5 \mu\text{m}$ ) in both simple compression and flexure tests, and compared the results with those of coarse-grained  $\text{Ti}_3\text{SiC}_2$  ( $100\text{-}200 \mu\text{m}$ ). These tests were conducted in the  $25\text{-}1300^\circ\text{C}$  temperature range. At ambient temperature, both the fine-grained and coarse-grained microstructures exhibited excellent damage tolerant properties. In both cases, the failure is brittle up to about  $1200^\circ\text{C}$ . At  $1300^\circ\text{C}$ , both microstructures exhibited plastic deformation ( $> 20\%$ ) in both flexure and compression. The fine-grained material exhibited higher strength compared to the coarse-grained material at all temperatures. Although the coarse-grained material was not susceptible to thermal shock (up to  $1400^\circ\text{C}$ ), the fine-grained material was found to thermal shock gradually between  $750^\circ\text{C}$  and  $1000^\circ\text{C}$ . The results presented herein provide evidence for two key aspects of the mechanical behavior of  $\text{Ti}_3\text{SiC}_2$ : (a) inelastic deformation entails basal slip and damage formation in the form of voids, grain boundary cracks, kinking and delamination of individual grains, and, (b) the initiation of damage does not result in catastrophic failure because  $\text{Ti}_3\text{SiC}_2$  can confine the spatial extent of the damage. This work was

published in the Journal of the American Ceramic Soc. in Oct. 1999. A reprint is attached to the end of this report.

- iii) In this work, large-grained, oriented, polycrystalline samples of  $\text{Ti}_3\text{SiC}_2$  loaded in compression at room temperature were shown to deform plastically [3]. When the basal planes were oriented in such a way that allowed for slip, deformation occurs by the formation of shear bands. The minimum critical resolved shear stress at room temperature is  $\approx 36$  MPa. When the slip planes are parallel to the applied load - a situation where ordinary glide is impossible - deformation occurs by a combination of delamination of, and kink band formation in individual grains, as well as shear band formation. It is this unique multiplicity of deformation modes that allows the material to deform plastically in any arbitrary orientation.

- Abstract iv) WAS The evolution of deformation-microfracture damage below Hertzian contacts in a coarse-grain  $\text{Ti}_3\text{SiC}_2$  is studied [4]. The Hertzian indentation stress-strain response deviates strongly from linearity beyond a well-defined maximum, with pronounced strain-softening, indicating exceptional deformability in this otherwise (elastically) stiff ceramic. Surface and subsurface ceramographic observations reveal extensive quasi-plastic microdamage zones at the contact sites. These damage zones are made up of multiple intragrain slip and intergrain shear failures, with attendant microfracture at high strains. No ring cracks or other macroscopic cracks are observed on or below the indented surfaces. The results suggest that  $\text{Ti}_3\text{SiC}_2$  may be ideally suited to contact applications where high strains and energy absorption prior to failure is required. This work was published in the Journal of the American Ceramic Soc. in Jan. 1998. A reprint is attached to the end of this report.

- Abstract v) WAS The ternary carbide,  $\text{Ti}_3\text{SiC}_2$ , fabricated by a reactive hot press route is investigated by transmission electron microscopy, TEM [5]. The material consists mainly of large elongated grains with planar boundaries and is characterized by a low defect density. Dislocations are observed in the grains and at grain boundaries. Perfect dislocations with  $\mathbf{b} = 1/3 \langle 11\bar{2}0 \rangle$  lying in (0001) basal planes are present. These basal plane dislocations are mobile and multiply as a result of room temperature deformation. All the stacking faults observed lie in the basal planes. This work was published in the Journal of the American Ceramic Soc. in June 1998. A reprint is attached to the end of this report.

#### References:

- 1) T. El-Raghy and M. W. Barsoum, "Processing and Mechanical Properties of  $\text{Ti}_3\text{SiC}_2$ : Part I: Reaction Path and Microstructure Evolution", J. Amer. Cer. Soc., **82**, 2849-54 (1999).
- 2) T. El-Raghy, M. W. Barsoum, A. Zavaliangos and S. Kalidindi, "Processing and Mechanical Properties of  $\text{Ti}_3\text{SiC}_2$ , Part II: Mechanical Properties", J. Amer. Cer. Soc., *ibid.* 2855-2859.
- 3) M. W. Barsoum and T. El-Raghy, "Room Temperature Ductile Carbides", Met. Mat. Trans., **30A**, 363-369 (1999).
- 4) I. M. Low, S. K. Lee, B. Lawn and M. W. Barsoum, "Contact Damage Accumulation in  $\text{Ti}_3\text{SiC}_2$ ", J. Amer. Cer. Soc., **81**, 225-28 (1998).
- 5) L. Farber, M. W. Barsoum, A. Zavaliangos, T. El-Raghy and I. Levin, "Dislocations and Stacking Faults in  $\text{Ti}_3\text{SiC}_2$ ", J. Amer. Cer. Soc., **81**, 1677-81 (1998).

# Processing and Mechanical Properties of $\text{Ti}_3\text{SiC}_2$ : I, Reaction Path and Microstructure Evolution

Tamer El-Raghy\* and Michel W. Barsoum\*

Department of Materials Engineering, Drexel University, Philadelphia, Pennsylvania 19104

In this article, the first part of a two-part study, we report the reaction path and microstructure evolution during the reactive hot isostatic pressing of  $\text{Ti}_3\text{SiC}_2$ , starting with titanium, SiC, and graphite powders. A series of interrupted hot isostatic press runs have been conducted as a function of temperature (1200–1600°C) and time (0–24 h). Based on X-ray diffractometry and scanning electron microscopy, at 1200°C, the intermediate phases are  $\text{TiC}_x$  and  $\text{Ti}_5\text{Si}_3\text{C}_x$ . Fully dense, essentially single-phase samples are fabricated in the 1450–1700°C temperature range. The time-temperature processing envelope for fabricating microstructures with small (3–5  $\mu\text{m}$ ), large (~200  $\mu\text{m}$ ), and duplex grains, in which large (100–200  $\mu\text{m}$ )  $\text{Ti}_3\text{SiC}_2$  grains are embedded in a much finer matrix, is delineated. The microstructure evolution is, to a large extent, determined by (i) the presence of unreacted phases, mainly  $\text{TiC}_x$ , which inhibits grain growth; (ii) a large anisotropy in growth rates along the  $c$  and  $a$  directions (at 1450°C, growth normal to the basal planes is about an order of magnitude smaller than that parallel to these planes; at 1600°C, the ratio is 4); and (iii) the impingement of grains.  $\text{Ti}_3\text{SiC}_2$  is thermally stable under vacuum and argon atmosphere at temperatures as high as 1600°C for as long as 24 h. The influence of grain size on the mechanical properties is discussed in the second part of this study.

## I. Introduction

TITANIUM SILICIDE ( $\text{Ti}_3\text{SiC}_2$ ) has an unusual combination of properties.<sup>1–7</sup> It is a better thermal and electrical conductor than titanium metal, quite resistant to thermal shock,<sup>1,2</sup> relatively light (4.5 g/cm<sup>3</sup>), and oxidation resistant.<sup>4</sup> Its hardness at 4 GPa is anomalously low for a carbide,<sup>1–3,7,9,10</sup> and, despite its excellent mechanical properties, it is readily machinable using regular high-speed tool steels; no cooling or lubrication is required. It recently has been shown that very-large-grained, oriented, polycrystalline samples of  $\text{Ti}_3\text{SiC}_2$  loaded in compression at room temperature deform plastically by a combination of shear- and kink-band formation.<sup>6</sup> The Hertzian indentation stress-strain response deviates from linearity beyond a well-defined maximum, with pronounced strain softening, indicating exceptional deformability.<sup>7</sup>

Although  $\text{Ti}_3\text{SiC}_2$  was first synthesized and its structure was determined in the late 1960s,<sup>8</sup> its potential as a useful structural high-temperature material was not appreciated mainly because of the difficulty of fabricating single-phase, bulk, polycrystalline samples. Some of the earlier work was conducted on chemically vapor deposited (CVD) samples.<sup>9,11,12</sup> It is in these

early reports that the anomalous nature of the hardness was first reported. Nickl *et al.*<sup>11</sup> noted that, although the CVD samples were soft, samples made via a solid-state reaction were not. Apart from two papers in which arch-melting was used,<sup>13,14</sup> in most cases, processing involved a two-step process where titanium, silicon, and carbon powders or TiC, silicon, and carbon mixtures were first reacted together to form a powder compact that was subsequently pulverized, and then hot pressed to yield polycrystalline samples.<sup>10,15–18</sup> These procedures, however, always led to mixtures of  $\text{Ti}_3\text{SiC}_2$ ,  $\text{TiC}_x$ , and  $\text{TiSi}_2$  and, sometimes,  $\text{Ti}_5\text{Si}_3\text{C}_x$  and/or SiC; the latter were some of the phases that are thermodynamically compatible with  $\text{Ti}_3\text{SiC}_2$ .<sup>14</sup> Some of the earlier work was hampered by the belief that  $\text{Ti}_3\text{SiC}_2$  dissociated at temperatures >1400°C and, consequently, could be processed only at lower temperatures.<sup>16–18</sup> As shown herein, this is a misconception:  $\text{Ti}_3\text{SiC}_2$  is stable and can be processed at temperatures as high as 1700°C.

The purpose of this study was to understand the reaction path and microstructure evolution during the processing of  $\text{Ti}_3\text{SiC}_2$  by a reactive hot isostatic pressing (HIPing) technique starting with titanium, SiC, and graphite. In the second part of the study, the effect of grain size on the mechanical properties was addressed.<sup>1</sup>

## II. Experimental Details

This work was conducted using high-purity powder mixtures of titanium (–325 mesh, 99.99% dehydrided; Alta Group, Golden, CO), SiC ( $d_m = 4 \mu\text{m}$ , 99.5%; Performance Ceramics, Peninsula, OH), and carbon ( $d_m = 1 \mu\text{m}$ , 99%; Aldrich Chemical Co., Milwaukee, WI) to yield a final composition with the appropriate stoichiometry. The powders were dry mixed in a V-blender for 2 h, and the mixture was cold pressed under 180 MPa into 69 mm × 12 mm × 12 mm bars. The bars then were encapsulated in Pyrex<sup>TM</sup> glass tubes under vacuum and placed in a HIP. The press was heated to 850°C at 10°C/min, under vacuum. At 850°C, enough argon was introduced into the HIP to yield a pressure of ~40 MPa. The HIP then was further heated at the same heating rate until the requisite temperature was reached. The processing temperature ranged from 1450° to 1700°C. The soaking times at temperature varied, but typically ranged from zero soak time (in which the HIP was turned off as soon as the requisite temperature was reached) to 24 h. Figure 1 summarizes the processing times and temperatures.

After HIPing, the samples were soaked in concentrated (48%) HF to dissolve the encapsulating glass (HF does not dissolve  $\text{Ti}_3\text{SiC}_2$ ), sliced using a diamond wheel, and polished using 1  $\mu\text{m}$  diamond suspension for microscopic evaluation. More than 15 runs were conducted (see Fig. 1). To expose the grains, the polished samples were etched using a 1:1:1 by volume HF:HNO<sub>3</sub>:H<sub>2</sub>O solution and observed under optical microscopy and scanning electron microscopy (SEM). X-ray diffractometry (XRD; scanning step (2 $\theta$ ) of 0.05° and a scanning rate of 0.1°/s; Model D-500, Siemens, Karlsruhe, Germany) was used for phase identification. A drill was used to obtain powders from the bulk of the samples for the XRD analysis.

P. F. Becher—contributing editor.

Manuscript No. 190250. Received April 20, 1998; approved March 15, 1999.  
Supported by U.S. Air Force Office of Scientific Research.  
\*Member, American Ceramic Society.

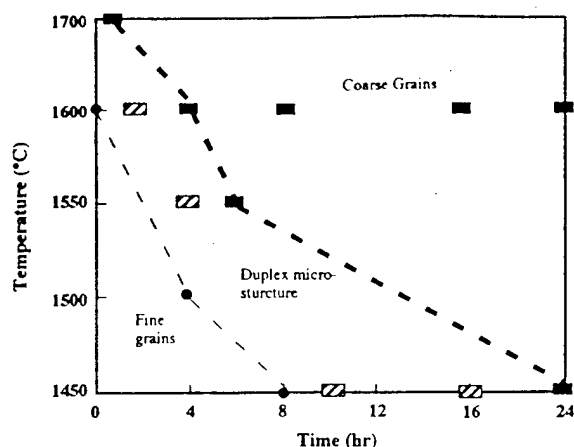


Fig. 1. Processing domains that result in the microstructures shown in Fig. 4. Fine, duplex, and coarse microstructures refer to Figs. 4(a), (b), and (c), respectively.

### III. Results and Discussion

#### (1) Reaction Path

The effect of time and temperature on the XRD patterns of the phases that formed as a result of heating in the HIP are summarized in Fig. 2. At 1200°C and no soak time, the main phases present are  $\text{TiC}_x$ ,  $\text{Ti}_5\text{Si}_3\text{C}_x$ , and some unreacted titanium. Some small peaks of  $\text{Ti}_3\text{SiC}_2$  are also visible. At 1400°C and no soak time, the major and minor phases are  $\text{Ti}_3\text{SiC}_2$  and  $\text{TiC}_x$ , respectively. Because the main peaks of  $\text{Ti}_3\text{SiC}_2$  overlap those of  $\text{Ti}_5\text{Si}_3\text{C}_x$ , it is not clear from the XRD data if the latter is present at that temperature. However, mass balance considerations dictate that  $\text{TiC}_x$  cannot be the only secondary phase present, because it contains no silicon. Furthermore, the presence of  $\text{Ti}_5\text{Si}_3\text{C}_x$  at 1400°C is confirmed by SEM. Figure 3(a) is a backscattered SEM micrograph of a polished but unetched cross section of a sample HIPed at 1400°C and furnace cooled. The dark phase is  $\text{Ti}_3\text{SiC}_2$ , and the light phase is  $\text{Ti}_5\text{Si}_3\text{C}_x$ . These phases have been confirmed by energy-dispersive X-ray (EDX) analysis. Figure 3(b) is a micrograph of a similar area after immersion in the etchant solution described above for 10 s. The appearance of the micrograph is not a surprise, because it is well established that HF readily dissolves silicides;<sup>12,13</sup> therefore,  $\text{Ti}_5\text{Si}_3\text{C}_x$  readily dissolves, leaving behind  $\text{Ti}_3\text{SiC}_2$ . This micrograph is important for another reason: it suggests that nucleation and growth of  $\text{Ti}_3\text{SiC}_2$  occurs within the  $\text{Ti}_5\text{Si}_3\text{C}_x$  phase.

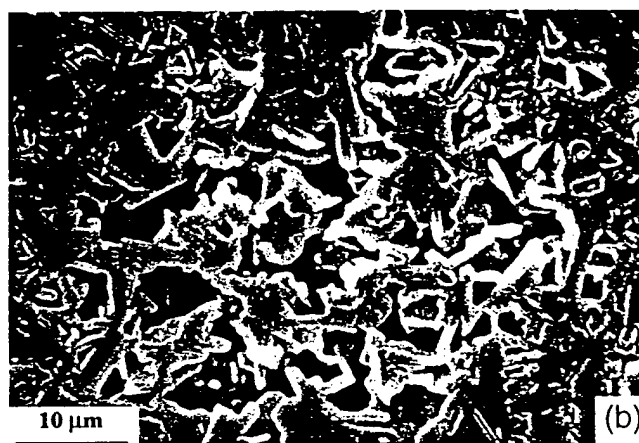


Fig. 3. (a) Backscattered SEM micrograph of sample heated to 1400°C and furnace cooled. Light phase is  $\text{Ti}_5\text{Si}_3\text{C}_x$  and dark phase is  $\text{Ti}_3\text{SiC}_2$ . (b) SEM micrograph of similar area after etching in solution for 10 s.  $\text{Ti}_5\text{Si}_3\text{C}_x$  phase is leached out, leaving only  $\text{Ti}_3\text{SiC}_2$ .

At 1600°C and no soak time, there is only a small amount (~5 vol%) of unreacted  $\text{TiC}_x$ . A 4 h hold at 1600°C removes the last vestiges of  $\text{TiC}_x$  and results in predominantly (>99%) phase-pure, fully dense samples. This has been corroborated with SEM backscattered images (not shown) in which the only phase present is  $\text{Ti}_3\text{SiC}_2$ . In some cases, 2 h at 1600°C is sufficient to obtain phase-pure materials.

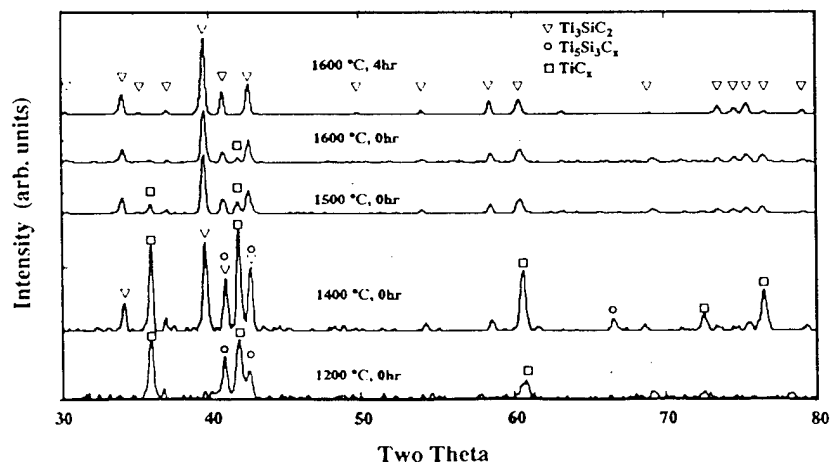


Fig. 2. PostHIPing XRD patterns of reaction products as a function of reaction temperatures and times ((□)  $\text{TiC}_x$ , (▽)  $\text{Ti}_3\text{SiC}_2$ , and (○)  $\text{Ti}_5\text{Si}_3\text{C}_x$ ).

SEM of the interrupted runs at 1200 °C (not shown here) clearly shows that the reaction mechanism is one in which carbon and silicon diffuse into the titanium particles forming  $TiC_1$  and  $Ti_4Si_3C_4$ . These phases, in turn, react to form  $Ti_3SiC_2$ . Given that  $TiC_1$  and  $Ti_4Si_3C_4$  are intermediate phases that react to form  $Ti_3SiC_2$ , an atomistic process wherein silicon diffuses out of the  $Ti_4Si_3C_4$  into  $TiC_1$ , concomitant with a counter diffusion of carbon out of the  $TiC_1$  into the  $Ti_4Si_3C_4$ , must be invoked (see Appendix A). Here it is assumed that the titanium atoms do not diffuse, which is an excellent assumption—given their size relative to the carbon or silicon atoms—that has been indirectly confirmed in our work on the silicidation and carburization of  $Ti_3SiC_2$ .<sup>19</sup> A similar conclusion has been reached by Brodtkin *et al.*,<sup>20</sup> who have shown that, during the heating of titanium,  $B_4C$ , and graphite powders, a reaction occurs first by the diffusion of carbon into the titanium at temperatures as low as 800 °C, followed by the decomposition of  $B_4C$  and diffusion of boron and carbon into the titanium and/or  $TiC_1$  particles to form  $TiB_2$  and  $Ti_3B_4$ .

The XRD results (Fig. 2) imply that the reaction path for the 3:1:2 composition starting with titanium, SiC, and graphite is  $Ti/TiC_1 + Ti_4Si_3C_4/Ti_3SiC_2/SiC$ . This conclusion is in agreement with the results of Wakelkamp *et al.*,<sup>14</sup> who have shown that the reaction products that form in a Ti–SiC diffusion couple, after a 100 h anneal at 1250 °C, are  $Ti/Ti_4Si_3C_4/Ti_3SiC_2 + TiC_1/Ti_3SiC_2/SiC$ . The phases in both cases are identical; their order, however, is slightly different. This difference is most likely attributable to the presence of graphite in our initial composition, which shifts the overall composition toward the carbon-rich corner to form  $TiC_1$  early in the reaction sequence. It is also instructive to compare the results obtained here with those obtained from Ti–SiC diffusion couples when the source of titanium is finite (i.e., when using titanium foils between SiC samples). In that case, the reaction products are  $Ti_3SiC_2$ ,  $TiSi_2$ , and/or  $Ti_4Si_3C_4$ .<sup>21,22</sup> In this work,  $TiSi_2$  has not been observed, again because of the presence of the graphite in the initial mix.

A not unrelated question is the thermal stability of  $Ti_3SiC_2$ . As noted above, more than one report exists in the literature claiming that  $Ti_3SiC_2$  dissociates at temperatures as low as 1450 °C.<sup>16–18</sup> To investigate the thermal stability of  $Ti_3SiC_2$ , bulk samples were annealed under vacuum ( $10^{-3}$  Pa) for 24 h at 1600 °C. In another experiment (–325 mesh)  $Ti_3SiC_2$  powders were annealed under argon at 1600 °C for up to 4 h. In both cases, XRD indicates that  $Ti_3SiC_2$  is the only phase present after the heat treatments. More important, the fact that some samples have been fabricated at 1700 °C is irrefutable evidence that  $Ti_3SiC_2$  is stable at that temperature.

## (2) Microstructure Evolution

The microstructure evolution study was conducted in the 1450°–1600 °C temperature range. The effect of soaking time at 1450 °C on the microstructure is shown in Fig. 4. After 8 h (Fig. 4(a)), the microstructure is uniform, with an average grain size of ~4 μm. After 16 h (Fig. 4(b)), a duplex microstructure, wherein ~100–200 μm platelike grains with an aspect ratio of ~8 are embedded in a much finer matrix, develops. After 24 h (Fig. 4(c)), the number of large grains has increased, and the microstructure is once again more uniform, with an average grain size of ~200 μm. The processing domains that result in the various microstructures are summarized in Fig. 1. Higher temperatures and time result in coarser-grained microstructures.

The micrographs in Fig. 4 show that  $Ti_3SiC_2$  exhibits anisotropic and abnormal or exaggerated grain-growth behavior. Various reasons have been proposed to explain this phenomenon: anisotropic surface energies for different crystal planes; layers of impurities or dopant ions on certain crystallographic planes that prevent growth in some directions; different wetting of anisotropic grains with liquid phases; and anisotropies in growth directions.<sup>23–25</sup>

The microstructural evolution can be understood if it is pos-

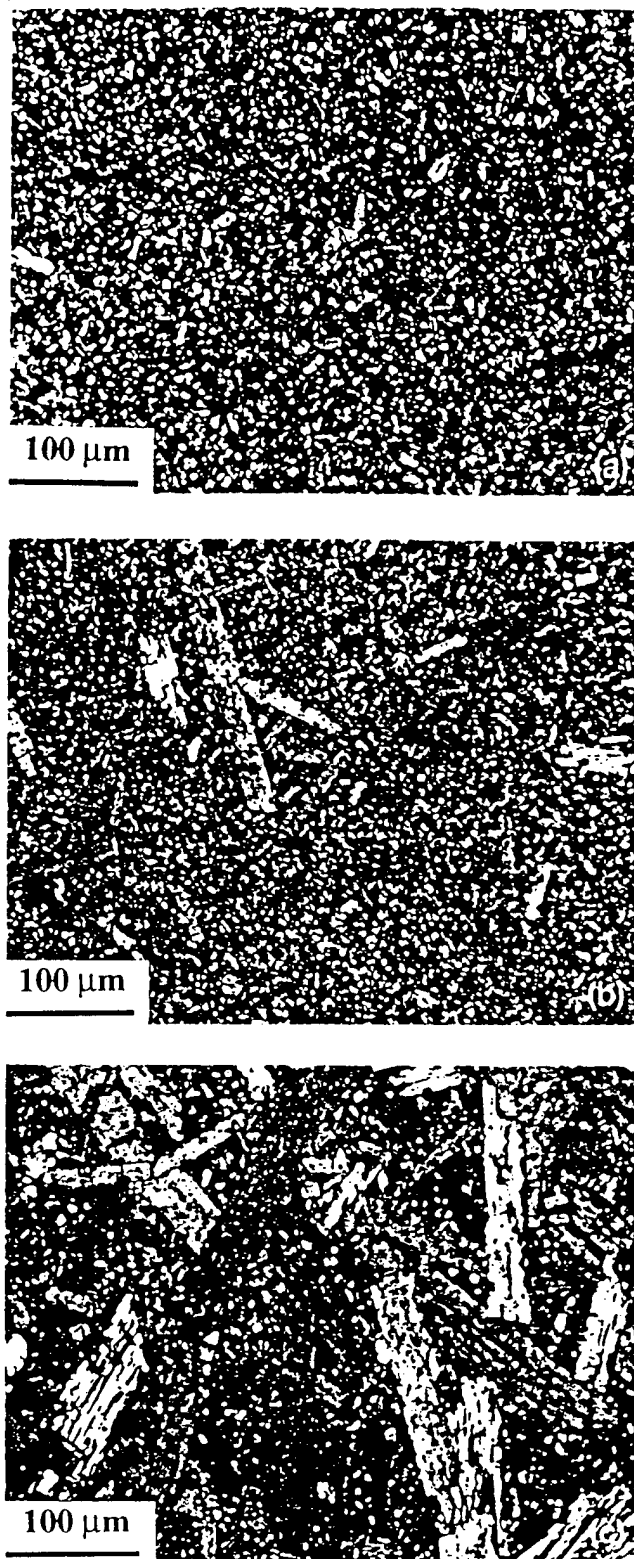


Fig. 4. Optical (unpolarized) micrographs of polished and etched samples HIPed at 1450 °C for (a) 8, (b) 16, and (c) 24 h

tulated that the unreacted  $TiC_1$  inhibits grain growth and that the grain-boundary mobilities normal to the basal planes are much higher than those parallel to these planes. The evidence for each postulate is discussed separately below.

To better appreciate the role of  $TiC_1$  on the microstructural evolution, we examined the microstructure of a sample that was hot pressed in a graphite die. Unlike the HIPed material, the hot-pressed samples contained sufficient  $TiC_1$ , especially

near the die walls, to observe its pinning effects. Figure 5(a) is a SEM micrograph of a cross section of a sample that was hot pressed in a graphite die for 24 h at 1600°C. Even after this extended high-temperature anneal, the size of grains adjacent to the  $\text{TiC}_x$  surface layer is  $\sim 10\text{--}20\text{ }\mu\text{m}$ . The presence of  $\text{TiC}_x$  (light phase) at some of the grain boundaries is obvious. Given that only a few of the grain boundaries shown in Fig. 5(a) are decorated by a distinct  $\text{TiC}_x$  phase and yet grain growth is impeded, it is suspected that  $\text{TiC}_x$  is present at most grain boundaries as well, but below the detectability limit of our instrument. We are currently conducting a transmission electron microscopy (TEM) study to explore this issue.

The micrograph shown in Fig. 5(b) is that of a sample that was hot-pressed for 4 h at 1600°C, but far removed from the die walls. Despite the significantly shorter time, the grains are much larger than in Fig. 5(a). These results are typical: grains in the vicinity of the graphite die walls never grow beyond the  $10\text{--}20\text{ }\mu\text{m}$  size, whereas those in the bulk typically grow to  $100\text{--}200\text{ }\mu\text{m}$  (Fig. 5(b)) after only 4 h at 1600°C. This correlation is so strong that we currently use the size of the grains after the high-temperature anneals as an indication of the lack or presence of  $\text{TiC}_x$  in the final microstructure; if they are present in sufficient concentrations, the grains do not grow larger than  $\sim 20\text{ }\mu\text{m}$ .

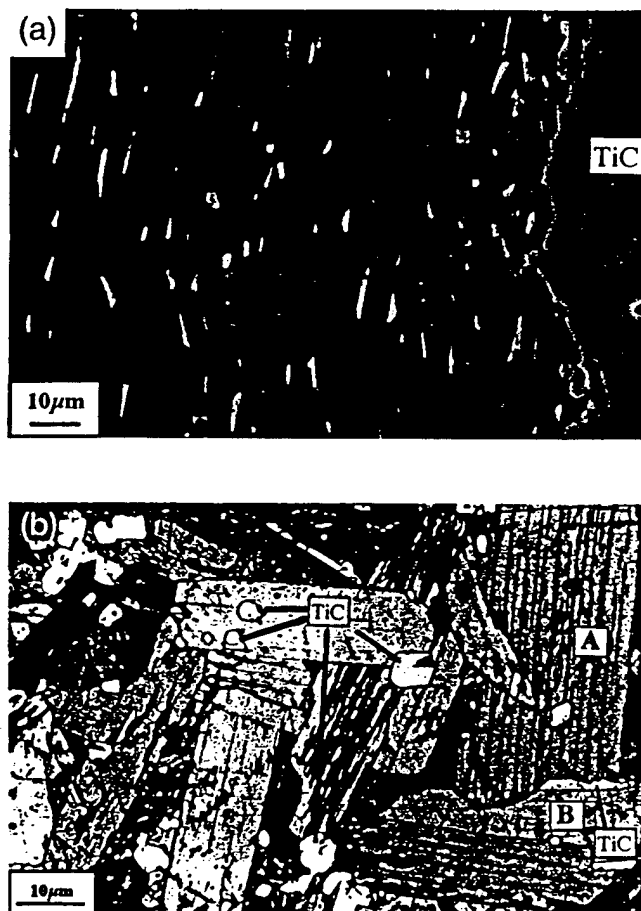


**Fig. 5.** Effect of  $\text{TiC}_x$  on grain growth of  $\text{Ti}_3\text{SiC}_2$ . (a) SEM micrograph of area adjacent to graphite foil that reacted with  $\text{Ti}_3\text{SiC}_2$  to form  $\text{TiC}_x$  (light phase). Sample was hot pressed for 24 h at 1600°C. (b) Optical micrograph taken near the center of a sample hot pressed for 4 h at 1600°C. Micrograph also shows the effect of  $\text{TiC}_x$  on grain-boundary mobility. Grain boundary of grain A, in which the basal planes are more or less vertical, is growing downward against its radius of curvature into the adjacent grain B. Sliver of  $\text{TiC}$  shown on right effectively blocks grain-boundary migration. (For a color reproduction of this micrograph, see cover of June 1997 issue of the *Journal of the American Ceramic Society*.)

More-direct evidence that  $\text{TiC}_x$  inhibits grain-boundary motion is shown in Fig. 5(b): the grain labeled A is growing downward into the adjacent grain labeled B. The growth front, however, is nonuniform and occurs only where  $\text{TiC}_x$  (white sliver cutting across the right-hand side of the boundary between grains A and B) is absent. This observation also explains how some of the  $\text{TiC}_x$  particles end up embedded in the  $\text{Ti}_3\text{SiC}_2$  grains: the latter simply grow around the former. In other micrographs (not shown here) we observe small  $\text{Ti}_3\text{SiC}_2$  grains that are totally embedded in much larger  $\text{Ti}_3\text{SiC}_2$  grains, as long as the smaller grains are sandwiched on either side by  $\text{TiC}_x$ . The latter observation also occurs in metallic systems.<sup>27</sup>

The onset of exaggerated grain growth at 1450°C and 1600°C coincides with the disappearance of the  $\text{TiC}_x$  peaks in the XRD patterns. In other words, the exaggerated grains start growing only when the reaction has proceeded far enough to reduce the concentration of  $\text{TiC}_x$  below a critical volume fraction. This conclusion is in total accord with a large body of literature on exaggerated grain growth in metals that has shown that the likelihood of exaggerated grain growth increases as the volume fraction of second phases at grain boundaries becomes vanishingly small (see, e.g., Ref. 26 and references therein).

A plot of the diameter,  $l$ , versus the widths,  $w$ , of isolated anisotropic grains (defined as grains that are not impinged on any side by other anisotropic grains, i.e., grains that are surrounded by fine grains only) is shown in Fig. 6(a) for two

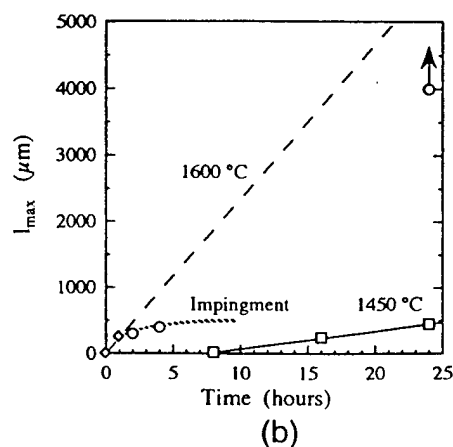
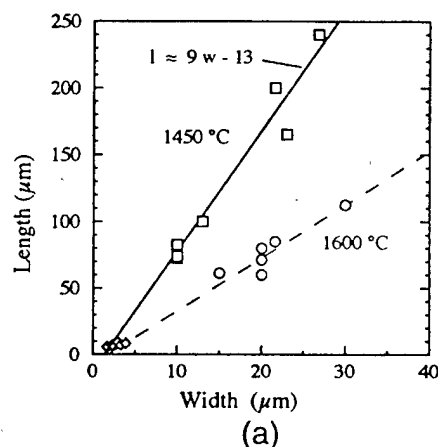


**Fig. 6.** (a) Diameter ( $l$ ) versus width ( $w$ ) of isolated (see text) anisotropic grains for sample HIPed at 1450°C for 16 h (see Fig. 4(b) for typical microstructure). Cluster of points in lower left-hand corner corresponds to grains in the samples annealed at 1450°C for 8 h (see Fig. 4(a)). (b) Time dependence of the maximum length ( $l_{\text{max}}$ ) of the exaggerated grains as a function of temperature. Impingement at 1600°C occurs in  $<2$  h. Circular points represent grains that have been impinged. Approximate growth rate at this temperature is given by the slope of the dashed line.

temperatures. A least-squares fit of the straight line for the 1450°C results yields a slope, i.e., an aspect ratio, of 9. The cluster of points shown in the lower left-hand corner corresponds to grains in the samples annealed at 1450°C for 8 h; in this regime there are no exaggerated grains and little correlation between  $w$  and  $l$ . A similar correlation between  $l$  and  $w$  exists for samples held at 1600°C for 1 h (dashed line in Fig. 6(a)). The aspect ratio in this case is  $4 \pm 0.5$ .

The time dependence of the diameters of the largest grain,  $l_{\max}$ , in a given microstructure is plotted in Fig. 6(b) as a function of temperature. At 1450°C (lower line), the points fall on a straight line with an intercept with the x-axis at  $\sim 7$  h, which is consistent with observations that anisotropic grains are rarely observed after 8 h anneals at 1450°C. Eight hours at 1450°C is also approximately the time at which the  $\text{TiC}_x$  peaks disappear in the XRD spectra. Combining the results shown in Figs. 6(a) and (b), the velocities at which the interfaces grow in the  $a$  and  $c$  directions are calculated to be  $15 \pm 1$  and  $1.6 \pm 0.1$   $\mu\text{m/h}$ , respectively. The results also imply a linear growth rate, which is expected, because the interfacial reaction kinetics *must* be rate limiting; in this single-phase material, diffusion does not play a role.

A plot of  $l_{\max}$  versus time at 1600°C is shown in Fig. 6(b). In contrast with the results at 1450°C,  $l_{\max}$  does not increase monotonically with time, but asymptotically converges to  $\sim 500$   $\mu\text{m}$  (hashed line labeled "impingement" in Fig. 6(b)). As discussed below, the variation of  $l_{\max}$  with time can be directly related to impingement. The largest grain after 1 h at 1600°C is 240  $\mu\text{m}$  (this point is not included in Fig. 6(a), because it is not an isolated grain). Combining these results with those in Fig. 6(a), the boundary velocities in the  $a$  and  $c$  directions at 1600°C are calculated to be  $\sim 120$  and  $30$   $\mu\text{m/h}$ , respectively. The rationale for using only the 1 h datum point and the origin to establish the boundary velocity is the following: At 1600°C and no hold, typically none of the grains are exaggerated. It follows that any line passing through the 1 h datum point should intersect positive values of the x-axis. The dashed line shown in Fig. 6(b) passes through the origin, and thus, the calculated velocity reported is a conservative number; the actual velocity is probably slightly higher. More supporting evidence is presented below.

The final grain size to which the exaggerated grains grow is determined by their impingement against each other. After a 2 h hold at 1600°C, most of the large grains have been impinged on by other anisotropic large grains. At longer times,  $l_{\max}$  reaches an asymptotic value of  $\sim 500$   $\mu\text{m}$ , as shown in Fig. 6(b) (hashed line). In support of this conclusion, we have shown that a forging operation early in the processing cycle aligns the grains.<sup>6</sup> Once aligned, the grains grow to millimeter sizes in a chevron pattern, as shown in Fig. 7. This sample was annealed at 1600°C for 24 h.<sup>6</sup> In these runs, the final grain size was limited by the thickness of the samples. The longest grains, however, were  $\sim 4$  mm.<sup>6</sup> This datum point is shown in Fig. 6(b) (top right) and is below the dashed line. Joining the first two data points (i.e., at 1 and 2 h) in Fig. 6(b) at 1600°C would

result in a line whose extension would lie below the 24 h point and intercept the x-axis at negative times. Similarly, the datum point at 1 h would be outside a line joining the 24 h point to the origin. These observations emphasize once again that (i) the use of the 1 h datum point to estimate the boundary velocity at 1600°C is valid and conservative, (ii) grain impingement is what determines the final grain length, and (iii) the exaggerated grains start growing at about the time 1600°C is reached. The latter conclusion is in accord with our XRD results and other microstructural observations.

The widths of the grains shown in Fig. 7 are significantly narrower than anticipated based on the boundary velocity estimated above. The aspect ratios are typically  $>20$ , and closer to 30. Once again, impingement of the anisotropic grains—an impingement between adjacent grains in this case—controls their width. Figure 7 shows that most of the boundaries formed appear to be low-angle grain boundaries; once formed, these boundaries do not migrate. The micrographs shown in Figs. 5(a) and 7 are of the same run, but different areas: Fig. 5(a) is of a region near the die walls and Fig. 7 is near the center of the sample.

Given the structure of  $\text{Ti}_3\text{SiC}_2$ , the anisotropy in growth is not too surprising. The layered nature of this material and the, presumably, atomic smoothness of the basal planes make it difficult for atoms to attach themselves to that interface, hence slowing their mobility. This problem is not unlike the growth of coherent precipitates normal to the habit planes in metallic systems.<sup>28-31</sup> In other words, the accommodation coefficients normal to habit planes are approximately zero, which, in turn, reduces the growth rates for precipitate thickening. The solution to the problem, first proposed by Aaronson,<sup>28</sup> and since verified,<sup>30,31</sup> is to form ledges or steps on the broad face of the precipitates. Atoms can then add to the riser of the ledge. Consistent with this picture is that the aspect ratio decreases with increasing temperature (Fig. 6(a)), presumably, as a result of the higher interface roughness at elevated temperatures.

The microstructure shown in Fig. 5(b) reveals that some of the large anisotropic grains grow into adjacent grains against their radii of curvature. For example, grain A in Fig. 5(b) is growing downward against its radius of curvature, which conclusively eliminates curvature as a driving force.

At this time, why some grains start to grow anisotropically is unclear and requires more work. This conclusion notwithstanding, it is instructive to compare the microstructures observed in this work with those of the two-dimensional Monte Carlo computer simulations of anisotropic grain growth in ceramics reported by Kunaver and Kolar.<sup>24</sup> In that work, a few anisotropic grains were embedded in a matrix of normally growing grains and allowed to grow. The anisotropic grains were assumed to have higher energies along one direction and lower energies along an orthogonal direction, relative to the average energy of the atoms in the fine-grained matrix. It was only by making that assumption that faceted anisotropic grains, not unlike the ones shown in Fig. 4(b), grew in the simulated microstructures.

The simulated microstructures and the microstructures shown here have some striking similarities, both in the overall time evolution of the microstructure and in many of the details. For example, in both microstructures, grains that grow against their radii of curvature and interpenetrate other abnormal grains are present. The simulations also show that the final microstructure is controlled by grain impingement, a conclusion that is in total accord with our observations. Although a simulation can never prove or disprove a given mechanism, the good qualitative agreement between the model and the experiment suggests that there is merit in the assumptions made by Kunaver and Kolar.<sup>24</sup>

#### IV. Summary and Conclusions

The reactive HIPing of titanium, SiC, and graphite powders is a viable technique to fabricate single-phase, fully dense,



Fig. 7. Optical (unpolarized) micrograph of polished and etched sample hot pressed at 1600°C for 24 h, after orienting the grains by forging.<sup>6</sup> This sample and the one shown in Fig. 5(a) are of the same run but different locations. Former was taken adjacent to the graphitic die wall. This micrograph is of an area near the center of the sample.

polycrystalline samples of  $\text{Ti}_3\text{SiC}_2$  with a variety of microstructures.  $\text{TiC}_x$  and  $\text{Ti}_5\text{Si}_3\text{C}_x$  are intermediate phases during the reaction, which implies that the reaction path is  $\text{Ti}/\text{TiC}_x/\text{Ti}_5\text{Si}_3\text{C}_x/\text{Ti}_3\text{SiC}_2/\text{SiC}$ . Dense, single-phase  $\text{Ti}_3\text{SiC}_2$  samples can be produced over a wide range of temperatures (1450–1700°C) and times (1–8 h, depending on temperature).  $\text{Ti}_3\text{SiC}_2$  exhibits exaggerated and anisotropic grain growth. At 1450°C, the grain-boundary mobility ratio parallel and normal to the basal planes is 9; at 1600°C the ratio decreases to 4.  $\text{TiC}_x$  reduces grain-boundary mobility. The growth of the anisotropic grains, and the coarsening of the microstructure in general, occurs only when the concentration of the  $\text{TiC}_x$  decreases below a certain critical level. Depending on time and temperature, three distinct microstructures can evolve: fine grained (3–5  $\mu\text{m}$ ), duplex (where coarse anisotropic grains are dispersed in a finer matrix), or coarse grained (100–200  $\mu\text{m}$ ).  $\text{Ti}_3\text{SiC}_2$  is thermally stable at temperatures as high as 1700°C under vacuum and argon atmospheres.

### Appendix A

Table AI outlines a possible reaction sequence to account for the reaction sequence outlined above. Initially, carbon diffuses into the titanium, forming  $\text{TiC}_{0.5}$  (reaction I). Simultaneously, silicon and carbon diffuse into titanium to form  $\text{Ti}_5\text{Si}_3\text{C}_x$  and reject carbon. Once these two phases are formed and if it is assumed that the titanium atoms do not diffuse into this system, silicon must diffuse out of  $\text{Ti}_5\text{Si}_3\text{C}_x$  to form  $\text{Ti}_3\text{SiC}_2$  (reaction III). This reaction sequence is not necessarily the one that occurs; the exact reaction sequence cannot be determined from our results. It is presented here more as an exercise that identifies what atoms have to diffuse through which phases to obtain  $\text{Ti}_3\text{SiC}_2$ . However, assuming only the diffusion of carbon and silicon atoms, this is a valid model to describe the nucleation and growth of  $\text{Ti}_3\text{SiC}_2$  within the  $\text{Ti}_5\text{Si}_3\text{C}$  phase field.

Table AI. Proposed Reaction Sequence to Account for the Formation of  $\text{TiC}_x$  and  $\text{Ti}_5\text{Si}_3\text{C}_x$  during Reaction Synthesis

Reaction	Remarks
$\frac{4}{3}\text{Ti} + \text{C} \rightarrow \frac{4}{3}\text{TiC}_{0.5} + \frac{1}{3}\text{C}$	I Free carbon reacts with titanium, forming $\text{TiC}_{0.5}$
$\frac{5}{3}\text{Ti} + \text{SiC} \rightarrow \frac{1}{3}\text{Ti}_5\text{Si}_3\text{C} + \frac{2}{3}\text{C}$	II SiC reacts with titanium, forming $\text{Ti}_5\text{Si}_3\text{C}$ and $\text{TiC}_{0.5}$ and rejecting carbon†
$\frac{4}{3}\text{TiC}_{0.5} + \frac{4}{9}\text{Si} + \frac{2}{9}\text{C} \rightarrow \frac{4}{9}\text{Ti}_3\text{SiC}_2$	III† Rejected atoms from reaction IV diffuse into $\text{TiC}_{0.5}$ , forming $\text{Ti}_3\text{SiC}_2$ and rejecting carbon
$\frac{1}{3}\text{Ti}_5\text{Si}_3\text{C} + \frac{7}{9}\text{C} \rightarrow \frac{5}{9}\text{Ti}_3\text{SiC}_2 + \frac{4}{9}\text{Si}$	IV† Rejected carbon atoms from reactions I, II, and III diffuse into $\text{Ti}_5\text{Si}_3\text{C}$ , forming $\text{Ti}_3\text{SiC}_2$ and rejecting silicon, which is used in reaction III
$3\text{Ti} + \text{SiC} + \text{C} \rightarrow \text{Ti}_3\text{SiC}_2$	Net overall reaction

†For the sake of simplicity, x in  $\text{Ti}_5\text{Si}_3\text{C}_x$  is assumed to be 1.<sup>32</sup> †Reactions III and IV occur simultaneously.

**Acknowledgments:** The authors are grateful to Professor R. Doherty for many useful and illuminating discussions.

### References

1. T. El-Raghy, M. W. Barsoum, A. Zavaliangos, and S. Kalidindi, "Processing and Mechanical Properties of  $\text{Ti}_3\text{SiC}_2$ : II. Effect of Grain Size and Deformation Temperature," *J. Am. Ceram. Soc.*, **82** [10] 2855–60 (1999).
2. M. W. Barsoum and T. El-Raghy, "Synthesis and Characterization of a Remarkable Ceramic:  $\text{Ti}_3\text{SiC}_2$ ," *J. Am. Ceram. Soc.*, **79** [7] 1953–56 (1996).
3. T. El-Raghy, A. Zavaliangos, M. W. Barsoum, and S. Kalidindi, "Damage Mechanisms Around Hardness Indentations in  $\text{Ti}_3\text{SiC}_2$ ," *J. Am. Ceram. Soc.*, **80**, 513–16 (1997).
4. M. W. Barsoum, T. El-Raghy, and L. Ogbuji, "Oxidation of  $\text{Ti}_3\text{SiC}_2$  in Air," *J. Electrochem. Soc.*, **144**, 2508–16 (1997).
5. M. W. Barsoum and T. El-Raghy, "A Progress Report on  $\text{Ti}_3\text{SiC}_2$ ,  $\text{Ti}_3\text{GeC}_2$ , and the H-Phases,  $\text{M}_2\text{BX}$ ," *J. Mater. Synth. Process.*, **5**, 197–216 (1997).
6. M. W. Barsoum and T. El-Raghy, "Room-Temperature Ductile Carbides," *Mater. Mater. Trans.*, **30A**, 363–69 (1999).
7. I. M. Low, S. K. Lee, B. Lawn, and M. W. Barsoum, "Contact Damage Accumulation in  $\text{Ti}_3\text{SiC}_2$ ," *J. Am. Ceram. Soc.*, **81**, 225–28 (1998).
8. W. Jeitschko and H. Nowotny, "Die Kristallstruktur von  $\text{Ti}_3\text{SiC}_2$ —Ein Neuer Komplexcarbidge-Typ," *Monatsh. Chem.*, **98**, 329–37 (1967).
9. T. Goto and T. Harai, "Chemically Vapor Deposited  $\text{Ti}_3\text{SiC}_2$ ," *Mater. Res. Bull.*, **22**, 1195–202 (1987).
10. R. Pampuch, J. Lis, L. Stobierski, and M. Tymkiewicz, "Solid Combustion Synthesis of  $\text{Ti}_3\text{SiC}_2$ ," *J. Eur. Ceram. Soc.*, **5**, 283 (1989).
11. J. J. Nickl, K. K. Schweitzer, and P. Luxenberg, "Gasphasenabscheidung im Systeme Ti-C-Si," *J. Less-Common Met.*, **26**, 283 (1972).
12. C. Racault, F. Langlais, R. Naslain, and Y. Kihn, "Chemically Vapor Deposition of  $\text{Ti}_3\text{SiC}_2$  from  $\text{TiCl}_4$ - $\text{SiCl}_4$ - $\text{CH}_4$ - $\text{H}_2$  Gas Mixtures," *J. Mater. Sci.*, **29**, 3941–48 (1994).
13. S. Arunajatesan and A. H. Carim, "Synthesis of Titanium Silicon Carbide," *J. Am. Ceram. Soc.*, **78**, 667 (1995).
14. W. J. J. Wakelkamp, F. J. van Loo, and R. Metselaar, "Phase Relations in the Titanium-Silicon-Carbon System," *J. Eur. Ceram. Soc.*, **8**, 135 (1991).
15. R. Pampuch, J. Lis, J. Piekarczyk, and L. Stobierski, "Solid Combustion Synthesis of  $\text{Ti}_3\text{SiC}_2$ ," *J. Mater. Synth. Process.*, **1**, 93 (1993).
16. J. Lis, Y. Miyamoto, R. Pampuch, and K. Tanihata, " $\text{Ti}_3\text{SiC}_2$ -Based Materials Prepared by HIP-SHS Techniques," *Mater. Lett.*, **22**, 163–68 (1995).
17. C. Racault, F. Langlais, and R. Naslain, "Solid-State Synthesis and Characterization of the Ternary Phase  $\text{Ti}_3\text{SiC}_2$ ," *J. Mater. Sci.*, **29**, 3384–92 (1994).
18. T. Okano, T. Yano, and T. Iseki, "Synthesis and Mechanical Properties of  $\text{Ti}_3\text{SiC}_2$  Ceramic," *Trans. Met. Soc. Jpn.*, **14A**, 597 (1993).
19. T. El-Raghy and M. W. Barsoum, "Diffusion Kinetics of the Carburization and Silicidation of  $\text{Ti}_3\text{SiC}_2$ ," *J. Appl. Phys.*, **83**, 112–19 (1998).
20. D. Brodtkin, S. Kalidindi, M. W. Barsoum, and A. Zavaliangos, "Microstructural Evolution during Transient Plastic Phase Processing of Titanium Carbide-Titanium Boride Composites," *J. Am. Ceram. Soc.*, **79** [7] 1945–52 (1996).
21. T. Iseki, T. Yano, and Y-S Chung, "Wetting and Properties of Reaction Products in Active Metal Brazing of SiC," *J. Ceram. Soc. Jpn. (Int. Ed.)*, **97**, 47–51 (1990).
22. S. Morozumi, M. Endo, M. Kikuchi, and K. Hamajima, "Bonding Mechanism Between Silicon Carbide and Thin Foils of Reactive Metals," *J. Mater. Sci.*, **20**, 3976–82 (1985).
23. T. Fang, "Abnormal Grain Growth in Sintering Powder Compacts," *Scr. Metall.*, **22**, 9–11 (1988).
24. U. Kunaver and D. Kolar, "Computer Simulation of Anisotropic Grain Growth in Ceramics," *Acta Mater.*, **41** [8] 2255–63 (1993).
25. J. Rödel and A. Glaeser, "Anisotropy of Grain Growth in Alumina," *J. Am. Ceram. Soc.*, **72** [11] 3292–301 (1990).
26. S. Bennison and M. Harmer, "Grain-Growth Kinetics for Alumina in the Absence of a Liquid Phase," *J. Am. Ceram. Soc.*, **68** [1] C-22–C-24 (1985).
27. J. W. Martin, R. D. Doherty, and B. Cantor, *Stability of Microstructure in Metallic Systems*, 2nd ed.; p. 346. Cambridge University Press, Cambridge, U.K., 1997.
28. H. I. Aaronson, *Decomposition of Austenite by the Diffusional Processes*; p. 387. Wiley Interscience, New York, 1962.
29. R. D. Doherty, *Physical Metallurgy*; Ch. 15. Edited by R. W. Cahn and P. Haasen. Elsevier, Amsterdam, The Netherlands, 1996.
30. G. C. Weatherly and C. M. Sargent, "Electron Diffraction Contrast from Ledges at the Interfaces of Faceted  $\theta'$  Precipitates," *Philos. Mag.*, **22**, 1049 (1970).
31. G. C. Weatherly, "The Structure of Ledges at Plate-Shaped Precipitates," *Acta Metall.*, **19**, 181 (1971).
32. M. Naka, J. C. Feng, and J. C. Schuster, "Phase Reaction and Diffusion Path of the SiC/Ti System," *Mater. Mater. Trans.*, **28A** [6] 1385–90 (1997).

## Processing and Mechanical Properties of $\text{Ti}_3\text{SiC}_2$ : II, Effect of Grain Size and Deformation Temperature

Tamer El-Raghy,\* Michel W. Barsoum,\* Antonios Zavalangos, and Surya R. Kalidindi

Department of Materials Engineering, Drexel University, Philadelphia, Pennsylvania 19104

In this article, the second part of a two-part study, we report on the mechanical behavior of  $\text{Ti}_3\text{SiC}_2$ . In particular, we have evaluated the mechanical response of fine-grained (3–5  $\mu\text{m}$ )  $\text{Ti}_3\text{SiC}_2$  in simple compression and flexure tests, and we have compared the results with those of coarse-grained (100–200  $\mu\text{m}$ )  $\text{Ti}_3\text{SiC}_2$ . These tests have been conducted in the 25°–1300°C temperature range. At ambient temperature, the fine- and coarse-grained microstructures exhibit excellent damage-tolerant properties. In both cases, failure is brittle up to ~1200°C. At 1300°C, both microstructures exhibit plastic deformation (>20%) in flexure and compression. The fine-grained material exhibits higher strength compared with the coarse-grained material at all temperatures. Although the coarse-grained material is not susceptible to thermal shock (up to 1400°C), the fine-grained material thermally shocks gradually between 750° and 1000°C. The results presented herein provide evidence for two important aspects of the mechanical behavior of  $\text{Ti}_3\text{SiC}_2$ : (i) inelastic deformation entails basal slip and damage formation in the form of voids, grain-boundary cracks, kinking, and delamination of individual grains, and (ii) the initiation of damage does not result in catastrophic failure, because  $\text{Ti}_3\text{SiC}_2$  can confine the spatial extent of the damage.

### I. Introduction

RECENTLY, we have reported on the fabrication and characterization of fully dense, bulk, single-phase polycrystalline samples of  $\text{Ti}_3\text{SiC}_2$ .<sup>1–9</sup> This ternary compound exhibits a unique combination of properties. It is a layered material that is as machinable as graphite.<sup>2,5</sup> At the same time, coarse-grained (100–300  $\mu\text{m}$ ) samples of  $\text{Ti}_3\text{SiC}_2$  have been observed to be damage tolerant,<sup>3</sup> not susceptible to thermal shock,<sup>2</sup> and oxidation resistant.<sup>4</sup> This material exhibits brittle failure characteristics at room temperature, but is plastic at 1300°C with “yield” points of 300 and 100 MPa in compression and flexure, respectively.<sup>2,5</sup> The strains to failure at 1300°C in the coarse-grained  $\text{Ti}_3\text{SiC}_2$  typically are >20%, even in the flexure tests.<sup>5</sup> The coarse-grained  $\text{Ti}_3\text{SiC}_2$  exhibits a fracture toughness of ~6.0  $\text{MPa}\cdot\text{m}^{1/2}$  (which is excellent for a layered material<sup>3</sup>) and a hardness of 4 GPa (which is a function of indentation load<sup>2,3,7</sup>). The surface hardness can be significantly enhanced by reacting  $\text{Ti}_3\text{SiC}_2$  with carbon to form TiC surface layers; reaction with silicon, on the other hand, enhances the oxidation resistance and the surface hardness.<sup>6</sup> The Hertzian indentation stress-strain response on this material deviates strongly from

linearity beyond a well-defined maximum, with pronounced strain softening, indicating unusual deformability in an otherwise elastically stiff material.<sup>7</sup>

Apart from the work cited above, there are no other reports in the literature dealing with the mechanical properties of phase-pure, bulk, polycrystalline samples of  $\text{Ti}_3\text{SiC}_2$ . Some of the earliest work was conducted on chemically vapor deposited (CVD) single-crystal samples.<sup>10,11</sup> It is in these early reports that the hardness and anisotropy are first reported. There are many studies reporting the mechanical properties of  $\text{Ti}_3\text{SiC}_2$  samples containing various volume fractions of  $\text{TiC}_x$  and/or other titanium silicides.<sup>12–17</sup> Pampuch, Lis, and co-workers<sup>12–15</sup> have tested samples containing 10–20 vol% TiC, and they have reported Young’s and shear moduli to be 326 and 135 GPa, respectively.<sup>13</sup> They also measured the hardness of  $\text{Ti}_3\text{SiC}_2$ -TiC composites as a function of TiC content and estimated that the hardness of pure, polycrystalline  $\text{Ti}_3\text{SiC}_2$  to be ~4 GPa.<sup>14</sup> Most recently, they fabricated hot-pressed  $\text{Ti}_3\text{SiC}_2$ -TiC composites with ~15 vol% TiC and reported compressive and three-point bend strengths of  $1120 \pm 270$  and  $350 \pm 63$  MPa, respectively.<sup>15</sup> Okano and co-workers<sup>16,17</sup> studied bulk, 95% dense samples that contained some secondary phases ( $\text{TiC}_x$  and titanium silicides), and they reported a flexural strength of 580 MPa and a fracture toughness of 6.9  $\text{MPa}\cdot\text{m}^{1/2}$  at ambient temperature. Okano and co-workers reported large plastic deformation in samples tested at 1200°C, which they have attributed to the presence of a grain-boundary phase.

More recently, we have shown that very-large-grained (3–4 mm), oriented, polycrystalline samples of  $\text{Ti}_3\text{SiC}_2$  loaded in compression at room temperature deform plastically,<sup>8</sup> even when the basal planes are aligned parallel to the applied load. The deformation occurs by a combination of delamination of individual grains, and kink- and shear-band formation. It is this multiplicity of deformation modes that is responsible for the level of plastic strain observed. The kinking referred to here was first proposed by Orowan<sup>18</sup> to explain deformation modes in some hexagonal single crystals. Later Hess and Barrett<sup>19</sup> and Frank and Stroth<sup>20</sup> outlined how the creation of pairs of dislocations of opposite signs and their motion in opposite directions could account for the macroscopic observations. Hess and Barrett also reported that these kink bands would be expected only in those crystals that are not subject to twinning as a result of compressive stresses. This includes hexagonal metals or alloys having an axial *c/a* ratio >1.73. Thus, it is not surprising that  $\text{Ti}_3\text{SiC}_2$ , which is hexagonal with a *c/a* ratio of 5.76,<sup>21</sup> deforms via this mechanism.

Transmission electron microscopy (TEM) observations have confirmed that basal-plane dislocations multiply and are mobile at room temperatures.<sup>9</sup> Recently, a dislocation-based model that builds on earlier ideas of kink-band formation<sup>18–20</sup> has been presented to explain deformation in  $\text{Ti}_3\text{SiC}_2$ .<sup>22</sup> The basic elements of the model are shear deformation by dislocation arrays, cavitation, creation of dislocation walls and kink boundaries, buckling of grains or parts thereof, and delamination. Most important, the nature of the damage—which mostly occurs in the form of delaminations—is such that it remains

P. F. Becher—contributing editor

Manuscript No. 190251 Received April 20, 1998; approved April 17, 1999  
Supported by the U.S. Air Force Office of Scientific Research  
\*Member, American Ceramic Society

localized and bounded by the kink boundaries. It is this containment of damage that is important in endowing  $\text{Ti}_3\text{SiC}_2$ —and, by extension, related ternary carbides—with the damage-tolerant properties discussed herein.

Most, if not all, of the properties studies reported to date have been conducted on large-grained samples.<sup>2–8</sup> The purpose of this work is to study the effect of grain size on compressive and flexural strengths, and the thermal shock resistance of  $\text{Ti}_3\text{SiC}_2$  in the 25°–1300°C temperature range.

## II. Experimental Details

The procedures for fabricating  $\text{Ti}_3\text{SiC}_2$  samples with different grain sizes were discussed in Part I of this work.<sup>1</sup> Briefly, titanium, SiC, and graphite powders were reactively hot isostatically pressed (HIPed) at 1450° and 1600°C for 4 h to produce fine- and coarse-grained microstructures, respectively. For the sake of brevity, fine grained and coarse grained are henceforth abbreviated FG and CG. Typical microstructures are shown in Figs. 4(a) and (c) in Part I of this paper.<sup>1</sup> X-ray diffractometry (XRD) and scanning electron microscopy (SEM) of the samples fabricated at 1450°C showed that they contained ~3 vol% of  $\text{TiC}_x$ . The time at 1450°C was intentionally kept short (4 h) to ensure that the sample was free of abnormal grains, some of which are shown in Fig. 4(b) in Part I.<sup>1</sup> The presence of large grains, in an otherwise fine matrix, affected the measured strengths adversely.

After HIPing, the surfaces of the samples were machined to remove the layer contaminated by the glass or the HF used to dissolve the glass. Cubes, 2 mm × 2 mm × 2 mm, were machined using a fine-grit, high-speed diamond wheel for the room- and elevated-temperature compression tests. The bend bars were tested as machined; no beveling of the edges or other polishing was deemed necessary. The choice of cubic rather than the more-appropriate cylindrical samples for the compression experiments was made because of the ease of machining of the former. This resulted in a minor artificial increase in the stress to failure and a decrease in the apparent plasticity observed.

The specimens for the four-point bend tests and the thermal shock measurements conformed to ASTM C1161<sup>†</sup> type A (25 mm × 2 mm × 1.5 mm) samples. The flexure strength ( $\sigma$ ) was calculated using the following relation:

$$\sigma = \frac{3P(l_1 - l_2)}{2BW^2} \quad (1)$$

where  $P$  is the load at fracture, and  $l_1$  and  $l_2$  the outer and the inner spans, respectively. A SiC fixture with an outer span of 20 mm and an inner span of 10 mm was used.  $B$  is the specimen width (2 mm) and  $W$  the specimen thickness (1.5 mm). The rollers were free to rotate but were not free to move in this setup. For tests where the specimen exhibited inelastic deformation,  $P$  was taken as the load at the onset of nonlinearity in the load–displacement curve (see Figs. 1(a) and (b)). Typically, three samples were used at each temperature and loading condition.

A servo-hydraulic testing machine (MTS Systems, Eden Prairie, MN) was used for all tests. The crosshead speed was 0.01 mm/s, which corresponds to a nominal strain rate of 0.005/s. All tests were conducted in air. The presence of a thin oxide layer, which never exceeded 100  $\mu\text{m}$ , was ignored in the stress calculations, and, consequently, the stresses reported here are underestimates of the actual stresses, especially at 1300°C, by as much as 10%.

The microhardness was measured (Model M-400, LECO

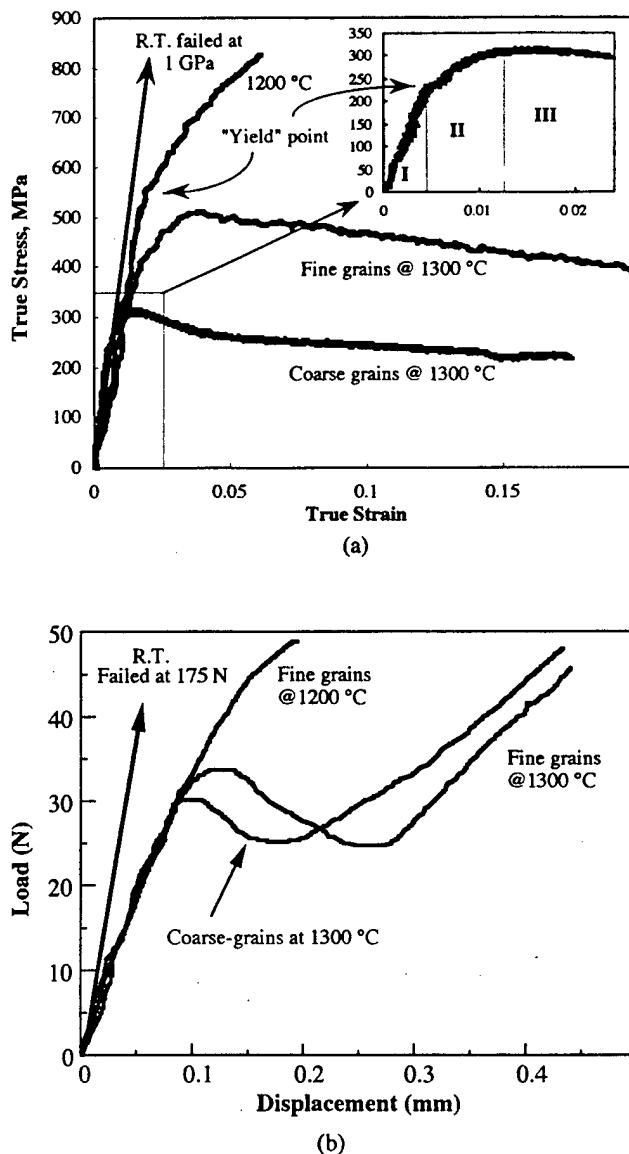


Fig. 1. Typical engineering stress–strain curves as a function of temperature and grain size in (a) compression and (b) four-point flexure. Unless otherwise noted, the curves are for the FG microstructure. In both cases, below 1200°C, the failure is brittle, whereas above 1200°C, the failure is plastic, with significant plasticity.

Co., St. Joseph, MI) at 0.5, 1, 5, and 10 N. The hardness was calculated by averaging at least 10 measurements at each load. To measure the damage tolerance, Vickers hardness indentations, using loads of 0.5, 5, 10, 100, and 300 N, were introduced on the tensile surface of the flexural samples, which were then loaded to failure. At least three samples were used at each indentation load.

For the thermal shock measurements, the furnace was preheated to the desired temperature ( $T_q$ ) and the cold samples were inserted, held at temperature for ~10 min, and quenched in ambient-temperature (25°C) water. The postquench retained flexural strengths were measured as a function of the severity of the quench, or  $\Delta T = T_q - T_{\text{water}}$ . Three samples were used for each quenching temperature.

## III. Results

Typical engineering stress–strain curves measured in compression are shown in Fig. 1(a) for three different temperatures

<sup>†</sup>Standard Test Method for Flexural Strength of Advanced Ceramics at Ambient Temperature, ASTM Designation C1161-94, American Society for Testing and Materials, West Conshohocken, PA.

**Table I. Effect of the Purity of SiC Starting Powders on Flexural and Compressive Strength<sup>†</sup>**

Temperature (°C)	Compression (MPa)		Four-point flexure (MPa)	
	Low-purity	High-purity	Low-purity	High-purity
25	600	720	260	320
1300	260	330	60	100

<sup>†</sup>Grains were large in both microstructures.

and the two grain sizes described earlier. Typical load-displacement data from the flexure tests are shown in Fig. 1(b). To convert the load-displacement data from the flexure tests to stress-strain data, we need reliable information on the post-yield<sup>†</sup> behavior of this material in tension and compression. The asymmetry between tension and compression is expected to result in a shift of the neutral axis. The quantitative relation between strength and damage evolution is a prerequisite for the interpretation of the bending results. Because this information is currently unavailable, we have presented the data from flexure tests in their raw form. We have, however, computed and reported values of flexure strength in Table I from this data using Eq. (1) and the load value at the deviation from the linear portion of the load-displacement curve.

In compression, below 1200°C, the stress-strain curve is linear to failure, with a failure stress that decreases with increasing grain size (Fig. 1(a)). At 1200°C, the permanent strain at failure is ~2.5%. No significant differences in the strains to failure at 1200°C are observed for the FG and CG microstructures. At 1300°C, significant levels of plastic strain are attained (Figs. 1(a) and (b)). The ends of the curves in Figs. 1(a) and (b) for the tests at 1300°C do not represent fracture; the tests were simply interrupted. In this work, the brittle-to-plastic transition temperature is defined as the temperature at which the strain to failure exceeds ~2%; it does not signify the activation of five independent slip systems. Recent results have shown that the temperature at which the transition occurs and the "yield" points in tension are functions of strain rate.<sup>23</sup>

The stress-strain response in simple compression at 1300°C (Fig. 1(a)) exhibits three stages (indicated by regions I, II, and III in the insert in Fig. 1(a)): (i) an elastic regime; (ii) a transient apparent "hardening" regime with a strong increase in stress over a small strain (80 MPa over 1% and 100 MPa over 2% for the CG and FG materials, respectively); and (iii) a distinct softening regime until the end of the test. The measured load-displacement plot for the flexure test at 1300°C (Fig. 1(b)) also exhibits a distinct softening regime (load-drop) followed by a regime in which the load increases significantly. Although this feature was highly repeatable in the flexure tests at 1300°C, it could have been an artifact of the experimental procedure.

The computed compressive and flexure strengths (using the load value at deviation from the linear portion of the data in Figs. 1(a) and (b)) for the FG and CG materials at different test temperatures are summarized in Figs. 2(a) and (b). At all temperatures, the FG material is stronger than the CG material, and the compressive strength is higher than the flexural strength. A large decrease in strength at ~1200°C is observed for FG and CG microstructures in compression and flexure.

Figure 3(a) summarizes the microhardness measurements for the FG and CG microstructures. At higher loads (100 N), the hardness is 4 GPa and independent of the grain size. The critical indentation load at which hardness becomes independent of the indentation load is influenced by the grain size and is typically larger for a larger-grain-sized material.

The measured values of the retained flexure strength after

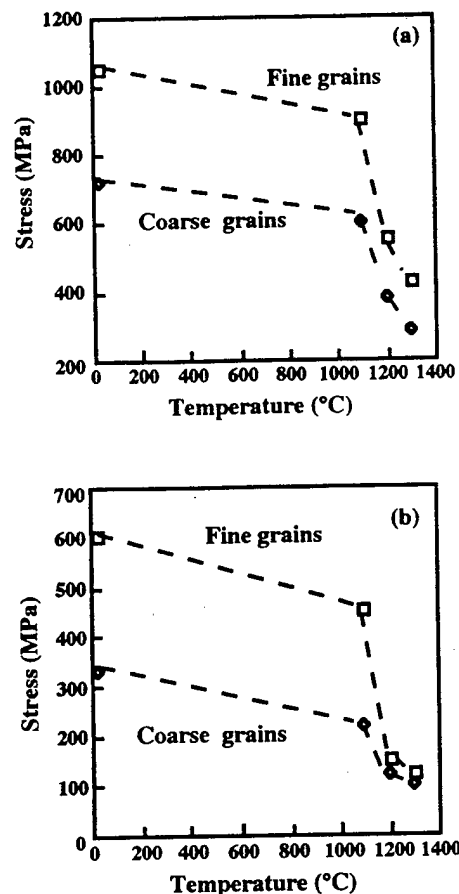


Fig. 2. Effect of grain size and temperature on (a) compressive strength and (b) flexural strength of  $Ti_3SiC_2$ .

the Vicker's indentations are summarized as a log-log plot in Fig. 3(b) for both microstructures. The hatched area on the left represents the strength of the samples as a result of natural flaws. In contrast with the FG material, for which the retained strength decreases immediately with increasing indentation load, the CG material exhibits a plateau at low loads.

Figure 4 summarizes the thermal shock resistance measurements for both the FG and CG samples. Although the CG samples are not susceptible to thermal shock (the data actually suggests a small increase in the post-thermal-shock flexure strength after quenching from 1400°C; see Fig. 4), the FG samples show a decrease in flexure strength of ~10% and 50% for a  $\Delta T$  of 750° and 1000°C, respectively.

#### IV. Discussion

As described in our previous work, CG samples of  $Ti_3SiC_2$  exhibit an unusual combination of properties.<sup>2-5</sup>  $Ti_3SiC_2$  exhibits plastic deformation at high temperatures, low hardness, damage tolerance, machinability, and thermal shock resistance,<sup>2</sup> and it exhibits brittle failure characteristics at room temperature, high Young's modulus, thermal stability, and oxidation resistance.<sup>2-6</sup> The results presented here confirm that most of these characteristics are also exhibited by the FG samples of  $Ti_3SiC_2$ , albeit at higher stress levels. The most significant difference in the overall mechanical behaviors of the FG and CG microstructures is in their thermal shock resistance properties. Figure 4 indicates that, although the CG samples are not susceptible to thermal shock, the FG samples are. However, unlike most carbides and silicides of titanium, the FG samples seem to thermal shock gradually over a 500°C temperature range. As discussed in more detail below, this is

<sup>†</sup>In this article, the term "yield stress" is used for the stress at which the stress-strain curve deviates from linearity. This stress level does not imply uniform plastic deformation due to crystallographic slip, but, rather, the initiation of damage, which, in turn, allows for inelastic deformation (see Discussion).

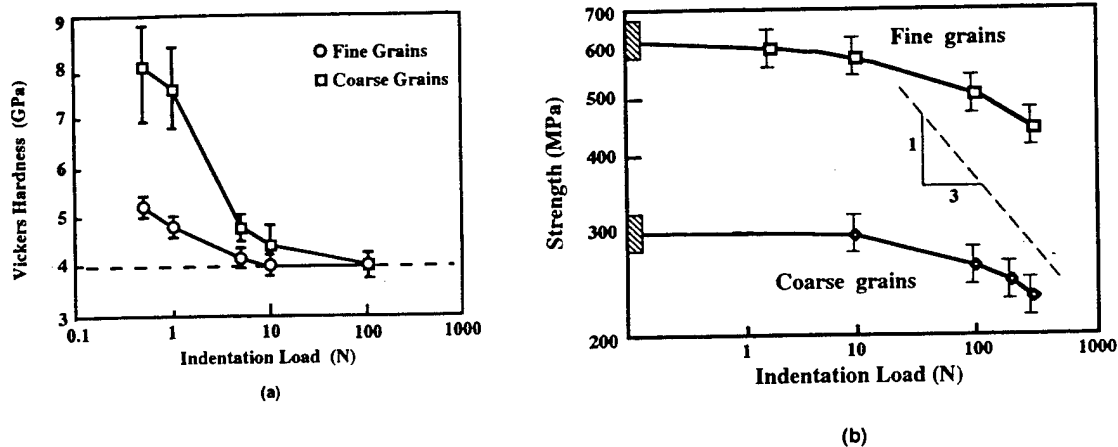


Fig. 3. (a) Effect of grain size on Vickers hardness as a function of applied load. For both microstructures, the asymptotic hardness value is 4 GPa. (b) Four-point flexural strength versus indentation load. Inclined dashed line has a slope of  $-1/3$ , which is the expected behavior for a perfectly brittle material.<sup>25</sup> Hatched area on the left represents the strength of the samples as a result of natural flaws.

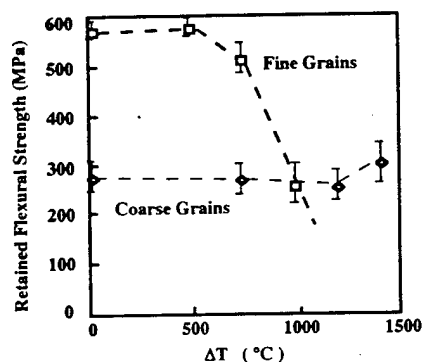


Fig. 4. Effect of grain size on thermal shock resistance. CG samples are not susceptible to thermal shock up to 1400°C. FG material thermal shocks between 750° and 1000°C.



Fig. 5. Optical micrograph of etched cross section of a sample deformed at 1300°C in compression. Grain denoted by the arrow buckled and delaminated into the void that formed to its right. Compression direction is vertical.

directly attributable to the damage tolerance exhibited by  $\text{Ti}_3\text{SiC}_2$ .

The data presented in Figs. 1 and 2 introduce some fundamental questions on the physical origin of the brittle-to-plastic transition that occurs at  $\sim 1200^\circ\text{C}$  in the CG and FG microstructures. This transition is attributable to potentially one of the following three sources, each of which is discussed in some detail below: (i) the activation of a new slip system, in addition to slip on the basal planes; (ii) an increase in the ease of kinking and accompanying lattice rotation of individual grains as a result of thermal activation; and (iii) the presence of small quantities of viscous grain-boundary films.

Based on preliminary transmission electron microscopy (TEM) observations on samples that were deformed at  $1300^\circ\text{C}$ , no evidence has been found for a second family of slip systems. However, because of the preliminary nature of the TEM observations, a second family of slip systems, although highly unlikely, cannot be totally ruled out at this time.

Given the critical role kinking and delamination of individual grains and the accompanying lattice rotations have in endowing oriented polycrystalline samples with considerable room-temperature plasticity, it is not unreasonable to assume that the same mechanisms are responsible for some of the readjustments needed in the polycrystals, especially at higher temperatures. Direct evidence for delamination and buckling during high-temperature compression of a polycrystalline sample is shown in Fig. 5. In this micrograph, the grain denoted by the arrow, by a combination of delamination and buckling, has been able to fill the cavity to its right that had been formed as a result of the mismatch of slip activity between neighboring

grains. This buckling and delamination must redistribute the strain and dissipate the stress concentration. The only deformation mode by which the cavity in Fig. 5 can be filled is the one shown, because the applied load direction is vertical; basal slip alone can never fill the cavity. Moreover, it has been shown previously (e.g., Fig. 13 in Ref. 5) that high-temperature compression of the CG material results in significant bending, rotation, and breakup of the individual grains, processes that can also result in cavity filling.

Kink- and shear-band formation and the delamination of individual grains have been readily observed at room temperature for (i) highly oriented samples when the latter are tested such that the basal planes are parallel to the applied load direction,<sup>8</sup> and (ii) grains that are confined by their surroundings.<sup>3,7</sup> Consequently, one would expect polycrystalline samples to be plastic at room temperature, when, in fact, they are not. One explanation for this apparent contradiction is to assume that the ease and, hence, extent of delamination and kinking are thermally activated, a reasonable assumption given that these processes entail the generation and motion of dislocations. The critical resolved shear stress of  $\text{Ti}_3\text{SiC}_2$  decreases from 36 MPa at room temperature to  $\sim 21$  MPa at  $1300^\circ\text{C}$ .<sup>8</sup> Considering the effect of temperature on the decrease in the overall stiffness (the shear modulus at  $1300^\circ\text{C}$  is  $\sim 80\%$  that at room temperature<sup>24</sup>), it is reasonable to assume that, at some temperature, the competition between fast fracture and stress

accommodation by kinking, buckling, and delamination changes in favor of the latter. That temperature is  $\sim 1200^\circ\text{C}$  for  $Ti_3SiC_2$ . As noted above, however, this temperature depends on the strain rate.

Figures 1(a) and (b) indicate fairly high slopes in the measured response after the initiation of inelastic deformation. This is especially apparent in the compression test, where the stress appears to increase from  $\sim 550$  to  $\sim 850$  MPa over a strain increment of  $\sim 0.05$  at  $1200^\circ\text{C}$ . Such exceedingly high hardening rates have not been reported, even for ductile metals and, thus, cannot account for these observations. An explanation that can be offered at this time is that damage initiates early in the elastic regime and results in plastic deformation, which is initially localized (i.e., not throughout the specimen). Further deformation is accomplished by additional damage development and plastic deformation. What is unusual is that the damage is not catastrophic. As noted above, the lack of five independent slip systems creates voids, which, in turn, cause kink bands and accompanying delaminations in their immediate vicinity. Further deformation leads to local, dislocation-based damage containment in the vicinity of these voids, which consequently redirects the damage to another location. In that respect, the behavior of  $Ti_3SiC_2$  is similar to a fiber-reinforced ceramic-matrix composite after the initiation of the first matrix crack.

Grain-boundary films also have been known to impart some limited plasticity to otherwise brittle materials at elevated temperatures. Such grain-boundary films by themselves do not impart the level of inelastic behavior observed in Fig. 1. However, a synergetic effect between grain-boundary films and the kink-based mechanism discussed above cannot be ruled out at this time. For example, we have previously shown that replacing the 99.5% pure SiC used in this study with a less-pure SiC (grit grade, 97.5%) affects the room- and high-temperature strengths of CG samples, as summarized in Table I. The influence (as a percentage change in property) is larger at the higher temperatures. The major impurities in the less-pure SiC are free silicon and  $SiO_2$ , both of which can form low-softening-point silicates at  $1300^\circ\text{C}$ . Consistent with this interpretation is that the oxidation resistance of the samples fabricated with the less-pure SiC are higher.<sup>4</sup> Therefore, it is conceivable, although unlikely, that the brittle-to-plastic transition observed in  $Ti_3SiC_2$  may be due, at least in part, to grain-boundary films that may be present in these microstructures. However, because one of the main advantages of reactive HIPing is the absence of sintering aids and other impurities that can be introduced during the making of powders, the role of grain-boundary films in the samples tested here should be minimal.

Because of the formation of median or Palmqvist cracks that emanate from the hardness indentations, the damage tolerance, as measured by the effect of the indentation loads on retained flexural strengths,<sup>24</sup> of brittle solids with fine microstructures is typically poor. In  $Ti_3SiC_2$ , these cracks are absent,<sup>3,7,13</sup> which partially explains its damage tolerance (Fig. 3(b)). It has been shown that CG  $Ti_3SiC_2$  is damage tolerant,<sup>3</sup> which is not deemed too unusual, because many CG ceramics are indeed damage tolerant.<sup>25</sup> What is rather surprising is the behavior of the FG microstructure shown in Fig. 3(b), in which the slope of the line is significantly less than the  $1/3$  slope one would expect from a brittle solid.<sup>25</sup> This is yet another manifestation of the extent by which damage localization is possible in this material. A more quantitative analysis would have to take into account the size of the plastic zone below the diamond indentation, the possibility of  $R$ -curve behavior, and the effect of load on the hardness (Fig. 3(a)), which, in turn, affects the size of the plastic zone.

The complexity of the problem also manifests itself in the effect of grain size on strength. Typically, the strengths of brittle solids scale with the inverse of the square root of the grain size. Making the same assumption here (i.e., assuming the grains are 10 and 100  $\mu\text{m}$  for the FG and CG microstructures, respectively), a strength ratio of  $\sim 3$  for the FG and CG microstructures is anticipated. The measured ambient tempera-

ture compressive and flexure strengths ratios are, however, in the range of 1.4–1.8. This is further evidence that the nature of damage in  $Ti_3SiC_2$  is different compared with the damage observed in more-brittle ceramics.

Consistent with this conclusion is the thermal shock resistance and its grain-size dependence. The CG samples do not appear to be susceptible to thermal shock, which implies that the flaws introduced by the quenching are smaller than the preexisting flaws in the material and that these preexisting flaws did not grow. The FG samples, on the other hand, are susceptible to thermal shock. The details of the damage evolution during thermal shock are outside the scope of this article and should be examined further.

## V. Conclusions

(i) In compression, room-temperature failure is brittle, with compressive strengths of 1050 and 720 MPa for the FG and CG materials, respectively. The compressive strengths decrease with increasing temperatures above  $1200^\circ\text{C}$ . At and below  $1200^\circ\text{C}$ , the failure is brittle, with strains to failure of  $<2\%$ . At  $1300^\circ\text{C}$ , both materials exhibit large plastic deformation levels ( $>20\%$ ), with yield points of 320 and 500 MPa for the CG and FG materials, respectively. Results presented here provide important evidence for two aspects of the mechanical behavior of  $Ti_3SiC_2$  reported earlier:<sup>2</sup> inelastic deformation in  $Ti_3SiC_2$  is assisted by damage formation in the form of grain boundary cracks, kinking, and delamination of grains; and initiation of damage does not result in catastrophic failure, because  $Ti_3SiC_2$  exhibits a capacity to confine the spatial extent of the damage.

(ii) At room temperature, the flexural strengths are 330 and 600 MPa for the CG and FG materials, respectively, and the failure is brittle. At  $1300^\circ\text{C}$ , associated with high levels of plastic deformation (deflection  $>1.5$  mm), yield points of 100 and 120 MPa are measured for the CG and FG materials, respectively.

(iii) FG and CG materials are damage tolerant.

(iv) Even though the CG material is thermal shock resistant up to  $1400^\circ\text{C}$ , the FG material loses its strength gradually: when quenched from  $750^\circ\text{C}$ , the strength decreases by  $\sim 10\%$ , and when quenched from  $1000^\circ\text{C}$ , it decreases to  $\sim 50\%$  of the prequench strength.

## References

- T. El-Raghy and M. W. Barsoum, "Processing and Mechanical Properties of  $Ti_3SiC_2$ : I, Reaction Path and Microstructure Evolution," *J. Am. Ceram. Soc.*, **82** (10) 2849–54 (1999).
- M. W. Barsoum and T. El-Raghy, "Synthesis and Characterization of a Remarkable Ceramic:  $Ti_3SiC_2$ ," *J. Am. Ceram. Soc.*, **79** (7) 1953–56 (1996).
- T. El-Raghy, A. Zavaliangos, M. W. Barsoum, and S. Kalidindi, "Damage Mechanisms Around Hardness Indentations in  $Ti_3SiC_2$ ," *J. Am. Ceram. Soc.*, **80**, 513–16 (1997).
- M. W. Barsoum, T. El-Raghy, and L. Ogbuji, "Oxidation of  $Ti_3SiC_2$  in Air," *J. Electrochem. Soc.*, **144**, 2508–16 (1997).
- M. W. Barsoum and T. El-Raghy, "A Progress Report on  $Ti_3SiC_2$ ,  $Ti_3GeC_2$ , and the H-Phases,  $M_2BX$ ," *J. Mater. Synth. Process.*, **5**, 197–216 (1997).
- T. El-Raghy and M. W. Barsoum, "Diffusion Kinetics of the Carburization and Silicidation of  $Ti_3SiC_2$ ," *J. Appl. Phys.*, **83**, 112–19 (1998).
- I. M. Low, S. K. Lee, B. Lawn, and M. W. Barsoum, "Contact Damage Accumulation in  $Ti_3SiC_2$ ," *J. Am. Ceram. Soc.*, **81**, 225–28 (1998).
- M. W. Barsoum and T. El-Raghy, "Room-Temperature Ductile Carbides," *Metall. Mater. Trans.*, **30A**, 363–69 (1999).
- L. Farber, M. W. Barsoum, A. Zavaliangos, T. El-Raghy, and I. Levin, "Dislocations and Stacking Faults in  $Ti_3SiC_2$ ," *J. Am. Ceram. Soc.*, **81**, 1677–81 (1998).
- J. J. Nickl, K. K. Schweitzer, and P. Luxenberg, "Gasphasenabscheidung im Systeme Ti-C-Si," *J. Less-Common Met.*, **26**, 283 (1972).
- T. Goto and T. Hirai, "Chemically Vapor Deposited  $Ti_3SiC_2$ ," *Mater. Res. Bull.*, **22**, 1195–202 (1987).
- R. Pampuch, J. Lis, L. Stobierski, and M. Tymkiewicz, "Solid Combustion Synthesis of  $Ti_3SiC_2$ ," *J. Eur. Ceram. Soc.*, **5**, 283 (1989).
- R. Pampuch, J. Lis, J. Piekarczyk, and L. Stobierski, "Solid Combustion Synthesis of  $Ti_3SiC_2$ ," *J. Mater. Synth. Process.*, **1**, 93 (1993).
- J. Lis, Y. Miyamoto, R. Pampuch, and K. Tanihata, " $Ti_3SiC_2$ -Based Materials by HIP-SHS Techniques," *Mater. Lett.*, **22**, 163–68 (1995).

- <sup>15</sup>T. Rudnik and J. Lis, "The  $\text{Ti}_3\text{SiC}_2$ -Based Structural Ceramics," *Arch. Metall.*, **42**, 59 (1997).
- <sup>16</sup>T. Okano, T. Yano, and T. Iseki, "Synthesis and Mechanical Properties of  $\text{Ti}_3\text{SiC}_2$  Ceramic," *Trans. Met. Soc. Jpn.*, **14A**, 597 (1993).
- <sup>17</sup>X. Tong, T. Okano, T. Iseki, and T. Yano, "Synthesis and High-Temperature Mechanical Properties of  $\text{Ti}_3\text{SiC}_2/\text{SiC}$  Composites," *J. Mater. Sci.*, **30**, 3078 (1995).
- <sup>18</sup>E. Orowan, "A Type of Plastic Deformation New in Metals," *Nature (London)*, **149**, 463–64 (1942).
- <sup>19</sup>J. B. Hess and C. S. Barrett, "Structure and Nature of Kink Bands in Zinc," *Trans. AIME*, **185**, 599–605 (1949).
- <sup>20</sup>F. C. Frank and A. N. Stroh, "On the Theory of Kinking," *Proc. Phys. Soc.*, **65**, 811–21 (1952).
- <sup>21</sup>W. Jeitschko and H. Nowotny, "Die Kristallstruktur von  $\text{Ti}_3\text{SiC}_2$ —Ein Neuer Komplexcarbidge-Typ," *Monatsh. Chem.*, **98**, 329–37 (1967).
- <sup>22</sup>M. W. Barsoum, L. Farber, T. El-Raghy, and I. Levin, "Dislocations, Kink Bands, and Room-Temperature Plasticity of  $\text{Ti}_3\text{SiC}_2$ ," *Metall. Mater. Trans.*, **30A**, 1727–38 (1999).
- <sup>23</sup>M. Radovic, M. W. Barsoum, T. El-Raghy, J. Seidensticker, and S. Wiederhorn, "Tensile Properties of  $\text{Ti}_3\text{SiC}_2$  in the 25°–1300°C Temperature Range," *Acta Mater.*, in press.
- <sup>24</sup>P. Finkel, M. W. Barsoum, and T. El-Raghy, "Low-Temperature Dependence of the Elastic Properties of  $\text{Ti}_3\text{SiC}_2$ ," *J. Appl. Phys.*, **85**, 7123–26 (1999).
- <sup>25</sup>R. F. Cook, B. R. Lawn, and C. J. Fairbanks, "Microstructure-Strength Properties in Ceramics: I, Effect of Crack Size on Toughness," *J. Am. Ceram. Soc.*, **68**, 604 (1985). □

Ti  
an  
zi  
ter  
tig  
tu  
sh  
an  
Sc  
str  
fr  
re  
fr  
pr  
ox

S  
cul  
oxi  
of  
SO  
res  
the  
per  
duc  
cha  
tan  
app  
tra  
stre  
isin  
dif  
the  
tiv  
dif  
sut  
cul  
ion  
Zr  
pro  
list  
Sc<sub>2</sub>

J.

M  
A

# Room-Temperature Ductile Carbides

M.W. BARSOUM and T. EL-RAGHY

Large-grained, oriented, polycrystalline samples of  $\text{Ti}_3\text{SiC}_2$  loaded in compression at room temperature deform plastically. When the basal planes are oriented in such a way that allows for slip, deformation occurs by the formation of shear bands. The minimum critical resolved shear stress at room temperature is  $\approx 36$  MPa. When the slip planes are parallel to the applied load—a situation where ordinary glide is impossible—deformation occurs by a combination of delamination of, and kink band formation in, individual grains, as well as by shear band formation. It is this unique multiplicity of deformation modes that allows the material to deform plastically in any arbitrary orientation.

## I. INTRODUCTION

CARBIDES are some of the hardest, stiffest, and most refractory materials known. The carbides of tungsten, silicon, and titanium, to name a few, all possess hardnesses in excess of 25 GPa and are thermally stable to at least 2000 °C. A notable exception is the ternary carbide  $\text{Ti}_3\text{SiC}_2$ , first synthesized over 30 years ago by Jeitschko and Nowotny,<sup>[1]</sup> who also determined its structure to be hexagonal with layers of TiC interleaved with hexagonal nets of Si. Later, Nickl *et al.*,<sup>[2]</sup> working with chemically vapor-deposited (CVD) films and small single crystals of  $\text{Ti}_3\text{SiC}_2$ , measured hardnesses that were quite low when compared to other carbides and were anisotropic (3 to 4 and 12 to 15 GPa, respectively, when tested parallel to and normal to the basal planes). They noted that their CVD samples showed unusual “plastic” behavior that was reminiscent of graphite. Later, Goto and Hirai,<sup>[3]</sup> also working with CVD samples, reconfirmed the earlier results and reported a hardness of 6 GPa. More recently, Pampuch and co-workers,<sup>[4,5,6]</sup> working with samples that contained at least 10 vol pct TiC, reported a Young’s modulus of 325 GPa and noted that, since the ratio of the hardness to the modulus was quite low, this somehow indicated that the material was plastic.

Most recently, the authors fabricated and characterized bulk, polycrystalline single-phase samples of  $\text{Ti}_3\text{SiC}_2$  as well as some of the closely related 211 phases or  $M_2BX$ , where  $M$  is a transition metal,  $B$  is a  $B$ -group element, and  $X$  is either carbon or nitrogen.<sup>[7–15]</sup> As a class, these carbides are good thermal and electrical conductors, relatively soft, with hardnesses in the range of 3 to 6 GPa, and machinable.<sup>[7–10]</sup> Furthermore,  $\text{Ti}_3\text{SiC}_2$  is damage tolerant, resistant to thermal shock,<sup>[7,11,13]</sup> relatively light (4.5 gm/cm<sup>3</sup>), elastically rigid, oxidation resistant, and stable up to at least 1700 °C.<sup>[12,14]</sup> Polycrystalline samples fail in a brittle manner at room temperature, but deform pseudoplastically at temperatures greater than 1200 °C.<sup>[13]</sup> At 1300 °C, the “yield” stresses (defined as the stress at which the stress-strain curve deviates from linearity) are 100 and 500 MPa in flexure and compression, respectively.<sup>[13]</sup> Atomistically, basal plane dislocations, with  $\mathbf{b} = 1/3 [11\bar{2}0]$ , multiply and are mobile at room temperature.<sup>[15]</sup>

In our work and that of others,<sup>[2–6]</sup> there have been some hints that the unusual combination of properties observed are somehow related to ambient temperature plasticity. For example, single buckled grains are easily identifiable in the vicinity of Vicker’s hardness indentations,<sup>[11]</sup> the material is softer and more damage tolerant than other carbides,<sup>[11,13]</sup> and it possesses the low hardness-to-modulus ratio alluded to previously.<sup>[5]</sup> The evidence to date, however, has been indirect. In this article, we present evidence for room-temperature plasticity in oriented, large-grained polycrystalline samples of  $\text{Ti}_3\text{SiC}_2$ . Just as important, we show that when the slip planes are parallel to the applied load, a situation where ordinary glide is impossible, a second distinct mechanism, namely, the kinking and delamination of individual grains occurs, which allows the material to deform plastically even in that orientation.

## II. EXPERIMENTAL DETAILS

Oriented macrograined (1 to 4 mm in length with aspect ratios of 20 to 40) polycrystalline samples were fabricated by a forging and grain-growth route. Titanium (99.99 pct, –325 mesh, provided by Alta Group (Arvada, CO), SiC (99.7 pct,  $d_m \approx 4$   $\mu\text{m}$ , provided by Performance Ceramics (Peninsula, OH)), and C powders (99 pct,  $d_m \approx 1$   $\mu\text{m}$ , provided by Aldrich Chemicals (Milwaukee, WI)) were weighed and dry mixed in a V-blender for 2 hours to yield the  $\text{Ti}_3\text{SiC}_2$  stoichiometry. The mixture was cold pressed into a  $76 \times 20 \times 25$  mm<sup>3</sup> green body, which, in turn, was placed in a vacuum furnace ( $1.3 \times 10^{-3}$  MPa), heated to 1450 °C at 10 °C/min, and held at that temperature for 8 hours. The resulting porous preform was single-phase  $\text{Ti}_3\text{SiC}_2$ , approximately 65 pct dense, with an average grain size of  $\approx 3$   $\mu\text{m}$ .

A  $15 \times 20 \times 25$  mm<sup>3</sup> billet was machined out of the preform and placed in a  $50 \times 25$  mm<sup>2</sup> channel graphite die that was presprayed with BN to prevent the sample from sticking to the die walls. The sample was placed in the die such that the hot- and cold-pressing directions coincided, and the 15-mm-long sample was centered in the 50-mm-long die channel. The width of the sample was identical to the width of the die, and its height was 20 mm. (The final height of the sample after deformation was  $\approx 4$  mm, for a total reduction in height of  $\approx 80$  pct.) The die was placed in the vacuum hot press and reheated to 1300 °C before applying any load. At that temperature, the preform was ductile and had enough strength that it did not crumble

M.W. BARSOUM, Professor, and T. EL-RAGHY, Research Assistant Professor, are with the Department of Materials Engineering, Drexel University, Philadelphia, PA 19104.

Manuscript submitted January 28, 1998.

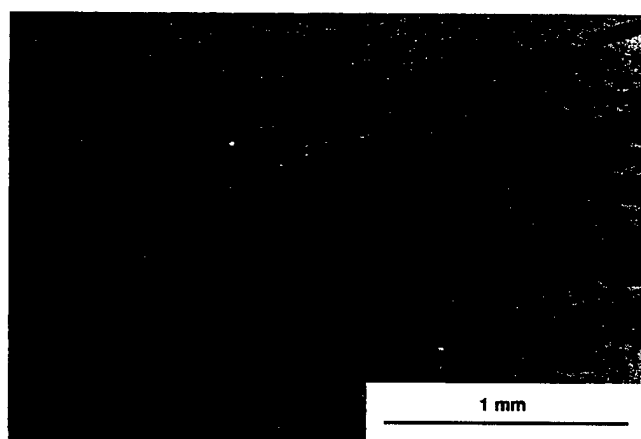
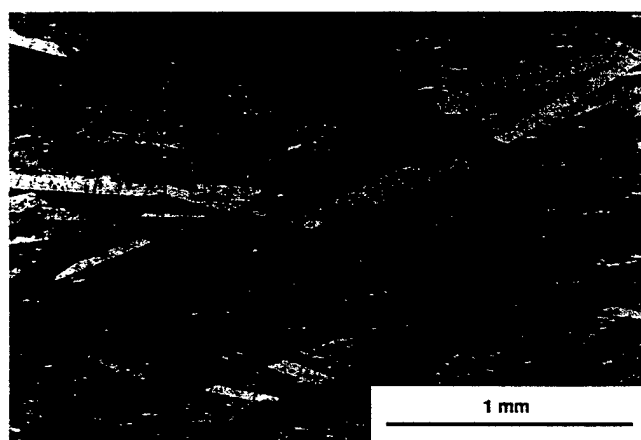
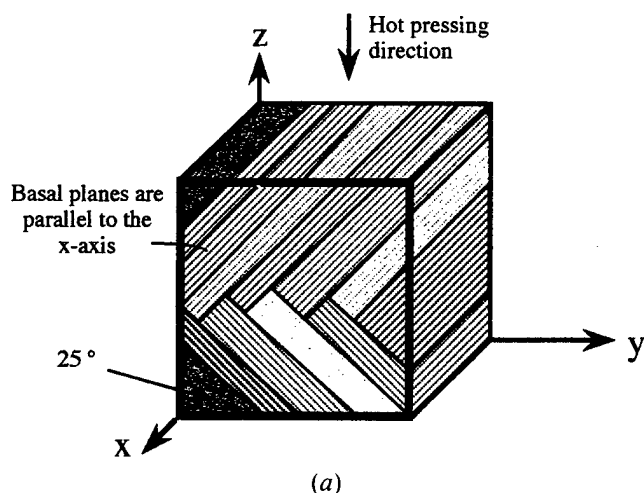


Fig. 1—(a) Schematic of grain orientation relative to loading directions. Basal planes are for the most part parallel to the  $x$ -axis. The hot pressing direction was vertical. Polished and etched optical micrograph of (b)  $y$ - $z$  plane and (c)  $x$ - $z$  plane.

upon application of the load. The load was then applied at a rate of 44.4 kN/h up to a load corresponding to a final stress (based on the die cross-sectional area) of 42 MPa. This stress was maintained for the duration of the run, while the sample was heated from 1300 °C to 1450 °C and was held at that temperature for 1 hour. This procedure allowed the sample to deform under nearly plane-strain conditions,

fill the die cavity, and densify, but was insufficient to cause much grain growth.<sup>[14]</sup> The sample was further heated to 1600 °C under load and held at that temperature for 24 hours. At this stage, the grains grow in the preferred orientation produced by the deformation to their final size. The relationship between the hot-pressing direction and the final grain orientation is depicted schematically in Figure 1(a).

The sample surfaces were machined off to remove the outer layers of TiC that formed as a result of C diffusion from the graphite die. Cubes measuring  $2 \times 2 \times 2$  mm<sup>3</sup> were machined for the compression tests. A servohydraulic MTS testing machine was preprogrammed to displace the platens at 0.01 mm/s to a given displacement, at which point the runs were interrupted; in other words, they were not run to failure. At least two samples were tested in each orientation at room temperature and at 1300 °C.

### III. RESULTS AND DISCUSSION

Optical micrographs of the polished and etched surfaces of the deformed cubes are shown in Figures 1(b) and (c), from which it is obvious that the grains are on the order of 1 to 2 mm in size and are highly oriented. Referring to Figure 1(a), the micrographs shown in Figures 1(b) and (c) are of the  $y$ - $z$  and  $x$ - $z$  planes, respectively. An X-ray diffraction of the  $y$ - $z$  plane showed that the intensity of the (110) reflections (*i.e.*, the prismatic planes) was enhanced by a factor of about 11 over what they would have been in a random sample. When taken together with the morphology of the fractured surfaces, which occur along the basal planes, there is little doubt that the grains are platelike and oriented such that their basal planes are parallel to the  $x$ -axis and intersect the  $x$ - $y$  plane at an angle of  $\approx 25$  deg, as shown schematically in Figure 1(a).

It is worth noting that, under identical processing conditions (*i.e.*, 1600 °C for 24 hours), randomly oriented grains, *i.e.*, in the absence of forging, will only grow to a final size of 100 to 400  $\mu$ m as they impinge on each other.<sup>[14]</sup> The forging operation rotates the grains while they are still fine, such that their fast-growing directions (*i.e.*, parallel to the basal planes) are parallel and in the direction of maximum shear. Once aligned, the grains grow to the millimeter sizes observed.

The compression tests were carried out along the  $x$ - and  $z$ -axes defined in Figure 1(a). A typical stress-strain curve for samples tested in the  $z$  direction is shown in Figure 2. The samples yielded around  $200 \pm 10$  MPa and deformed plastically thereafter until the test was interrupted. It is worth noting that it is possible to deform these samples in compression to strains that exceed 50 pct. At 1300 °C, the shape of the stress-strain curve (not shown) is similar to that at room temperature, but yields at the lower stress of  $120 \pm 10$  MPa.

As noted previously, transmission electron microscopy of undeformed and deformed samples of  $\text{Ti}_3\text{SiC}_2$  has shown that perfect dislocations with  $\mathbf{b} = 1/3 [11\bar{2}0]$  lying in the basal plane multiply and are mobile at room temperature.<sup>[15]</sup> To estimate the critical resolved shear stress, the angles between the loading direction and the slip planes and directions must be known. The former is  $\approx 65$  deg. The angle between the slip and the loading directions is unknown. Its maximum value, however, is when the slip direction,

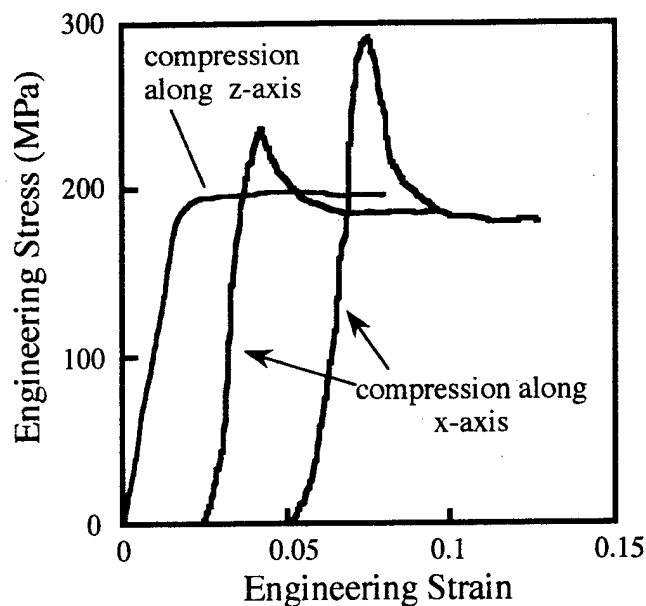


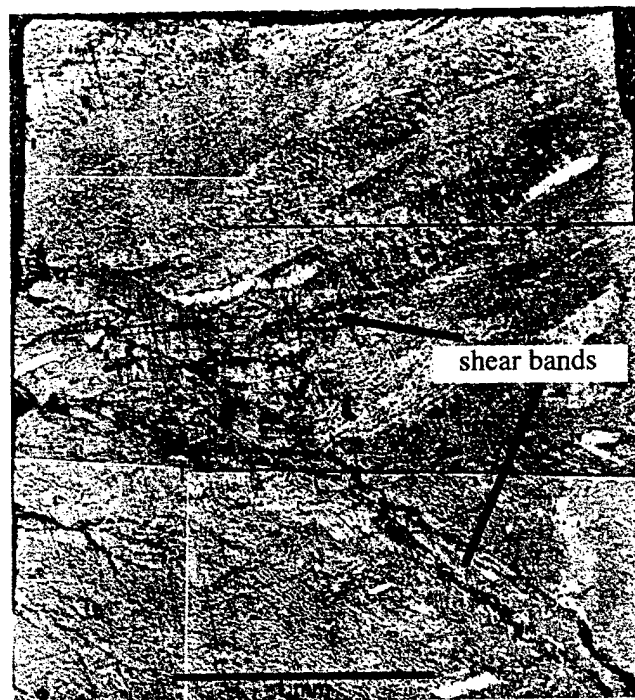
Fig. 2—Effect of  $\text{TiSiC}_2$  grain orientation on room-temperature engineering stress-strain curves compressed in the  $z$  directions and the  $x$  direction, i.e., parallel to the basal planes. The curves are shifted by 0.025 strain for clarity's sake.

$[11\bar{2}0]$ , is the same as the slip plane, viz., 65 deg. Thus, the minimum critical resolved shear stress at room temperature is  $\approx 36$  MPa. The corresponding value at 1300 °C is  $\approx 22$  MPa.

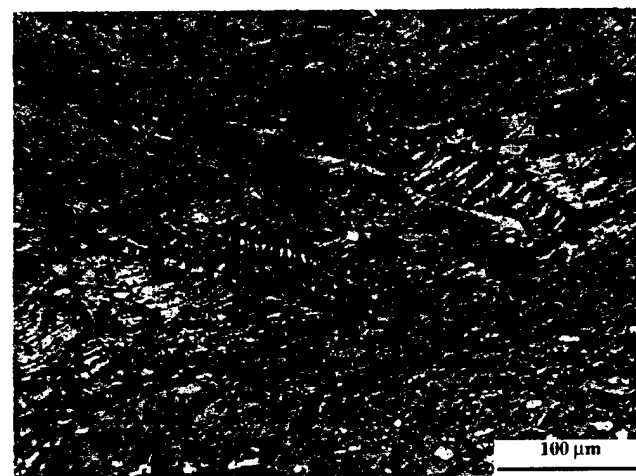
When compressed along the  $x$  direction, a clear maximum in the yield stress is observed, which is followed by a region of strain softening (Figure 2). Two nominally identical samples were tested; one sample yielded at 230 MPa and the second at 290 MPa. As discussed subsequently, the scatter and strain softening are consistent with the deformation mode proposed.

An optical micrograph of a sample compressed along the  $z$  direction is shown in Figure 3(a), from which it is obvious that the deformation is mostly confined to two intersecting shear bands that are parallel to the basal planes. The two bands intersect left of center, and their intersection results in the creation of cavities and pores (Figure 3(a)). Where the shear bands intersect the right-hand edge of the sample, a bulge is apparent, confirming the plastic nature of the deformation. At higher magnifications, the extensive deformation within the shear band, which is slightly wider than 100  $\mu\text{m}$ , is obvious (Figure 3(b)). Outside these bands, the material appears almost intact, at least at the magnification shown. Figure 3(b) indicates that grain rotation, grain breakup, and, possibly, twinning occurs within the shear band. These observations notwithstanding, it is hereby acknowledged that the details of the deformation mechanisms operative within the shear bands are unknown.

The postdeformation optical micrograph of a sample compressed along the  $x$  direction is shown in Figure 4(a). Here again, the deformation is mostly confined to two intersecting shear bands that form an inverted chevron shape. Where they intersect, a large void is present. In addition to the shear bands, there are a number of other features, the most important of which is the delamination and kinking observed at the lower left-hand corner (Figure 4(b)). This deformation mode is neither twinning nor regular glide, but



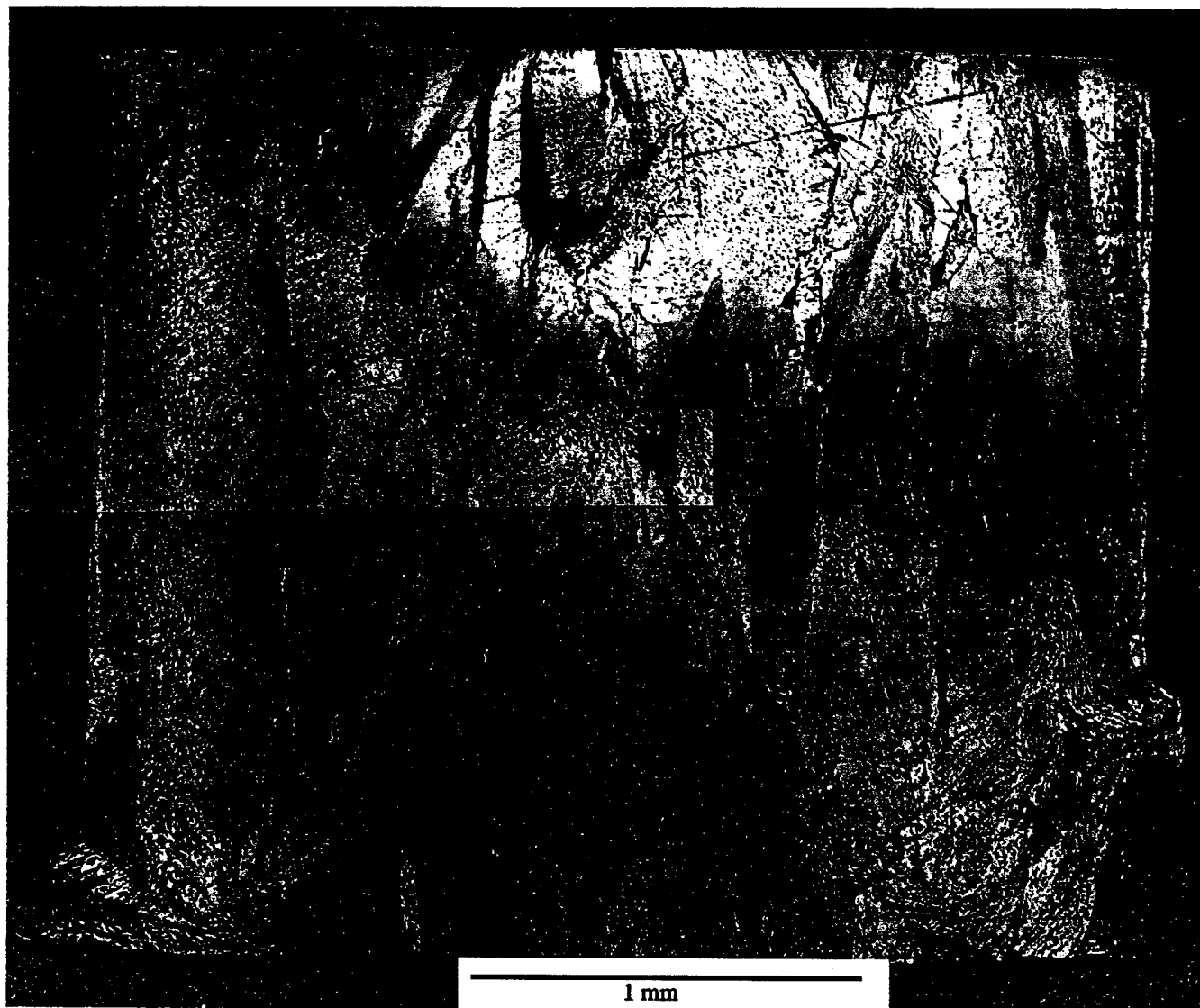
(a)



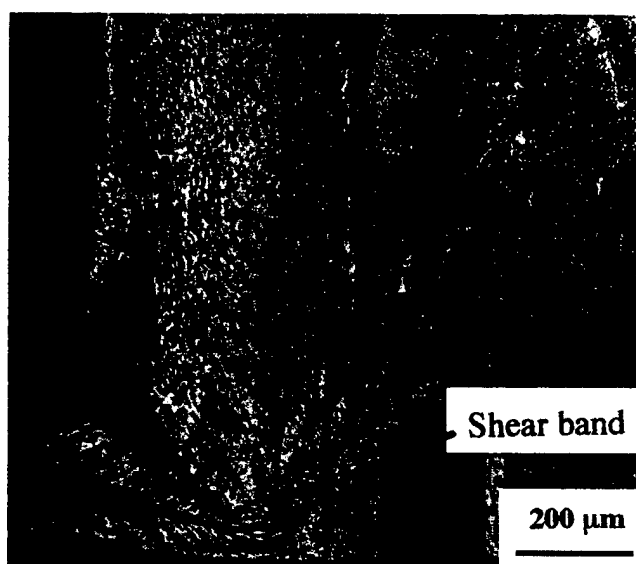
(b)

Fig. 3—(a) Polished and etched optical micrograph of the surface of a cube subjected to a 6 pct compressive strain. Basal planes make an angle of  $\approx 25$  deg with the horizontal; the load was applied vertically. Note the two intersecting shear bands. Outside the shear bands, the material appears to have remained intact. (b) Higher magnification optical micrograph of the shear band. Note extensive grain breakup, rotation, etc. within the band.

rather one of kink-band formation, first described by Orowan to explain kinking in some hexagonal single crystals.<sup>[16]</sup> These bands form by the rotation of parallel lamella, of approximately equal thickness, away from their original position, as illustrated in Figure 5(a). When a crystal bends and then becomes unstable, a region of highly localized deformation develops, whose boundaries with the relatively undeformed crystal are nearly normal to the slip planes and directions. Later, Hess and Barrett<sup>[17]</sup> outlined how the creation of pairs of dislocations of opposite signs, and their motion in opposite directions, could account for the macroscopic observations. Hess and Barrett also pointed out



(a)



(b)

Fig. 4.—(a) Polished and etched optical micrograph of the surface of a cube subjected to a 6 pct compressive strain. Basal planes are parallel to the vertically applied load. (b) Higher magnification of kinked lower left-hand corner.

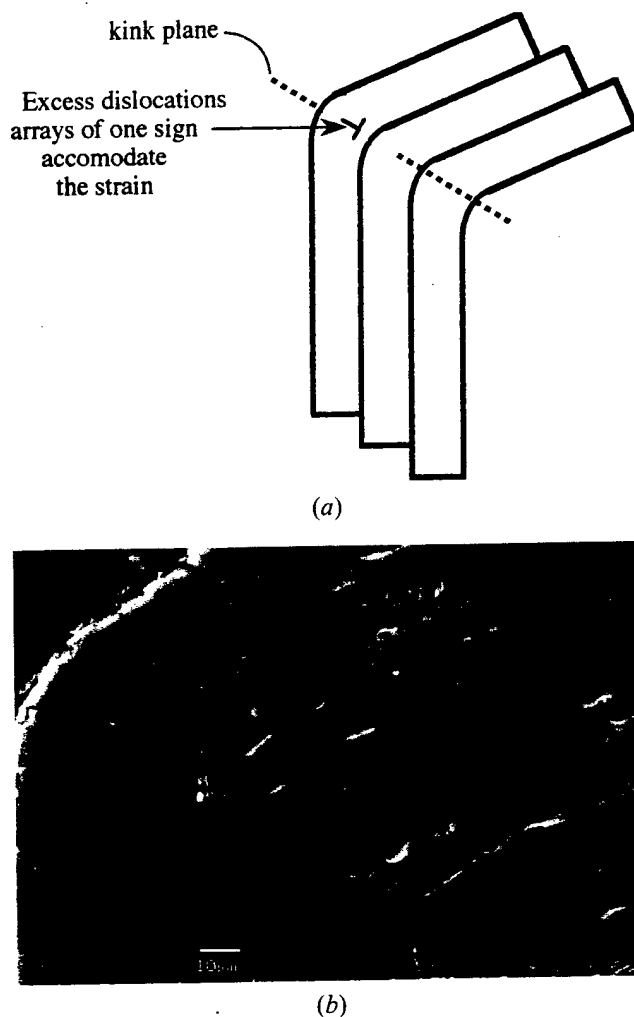


Fig. 5—Geometrical elements of a kink band according to Orowan.<sup>[16]</sup> The compression axis is vertical. (b) An SEM micrograph of the same general area as Fig. 4(b).

that these kink bands would be expected only in those crystals that are not subject to twinning as a result of compressive stresses. In other words, hexagonal metals or alloys having an axial  $c/a$  ratio greater than 1.73. It is, thus, not surprising that  $\text{Ti}_3\text{SiC}_2$ , which is hexagonal with a  $c/a$  ratio of 5.76, deforms *via* this mechanism.

That individual grains of  $\text{Ti}_3\text{SiC}_2$  kink and delaminate is obvious from the micrographs shown in Figures 4(b) and 5(b) and in our previous work.<sup>[11]</sup> This deformation mode has also been observed in some of the 211 phases.<sup>[8,9]</sup> Kinking and kink-band formation originate in materials with a strong anisotropy in their shear strengths when they are loaded such that the load is typically parallel to the slip or weak shear planes. This mechanism has been invoked to explain deformation in single-crystal hexagonal metals,<sup>[16,17,18]</sup> highly constrained rocks,<sup>[19]</sup> organic crystals,<sup>[20]</sup> card decks,<sup>[21]</sup> rubber laminates,<sup>[22]</sup> oriented polymer fibers,<sup>[23–27]</sup> wood,<sup>[28]</sup> graphite fibers,<sup>[29,30]</sup> laminated C-C and C-epoxy composites,<sup>[31,32,33]</sup> and highly textured Zn polycrystalline samples,<sup>[34]</sup> among others.

Figure 2 identifies strain-softening in  $\text{Ti}_3\text{SiC}_2$  to be a texture-related phenomenon. The simplest interpretation is that regions which prior to kinking could not deform by basal slip assume orientations in which basal slip is relatively

easy. Clear evidence for lattice rotation can be seen in the lower left-hand-side corner of (Figure 4(b)). The kinking reorients the basal planes in the kinked region to an angle that is slightly steeper than the angle between the shear band and the horizontal. The relationship between the angle that the shear and kink bands make with the horizontal is obvious. It is not clear at this time why the former angle at  $\approx 45^\circ$  is slightly steeper than the latter at  $30^\circ$ , but is probably related to the fact that the shear band is constrained, whereas kinking at the corner is not. As noted by Orowan, the plane of kinking need not be a crystallographic plane; its orientation depends on the stress condition.<sup>[16]</sup>

The kinking/delamination deformation mode is a result of an instability and a lack of constraints and, as such, is dependent on stochastic microstructural features such as imperfections, sharp corners, voids, planar misalignment, *etc.* The more than 22 pct difference in the values of the maximum stresses of the two nominally identical samples (Figure 2) is consistent with such a deformation mode. In contrast, the stress needed to further plastically deform the crystal, which presumably is dominated by what is occurring within the shear bands, is more or less constant and fairly reproducible (Figure 2). The combination of stress concentration and lack of constraint at the corners resulted in their kinking and delamination, which is why the two shear bands appear to have originated at the lower corners.

The general shapes of the stress-strain curves shown in Figure 2 are similar to those reported by Edwards *et al.*<sup>[34]</sup> and Tapetado and Loretto.<sup>[18]</sup> The latter have shown that if kinking in single crystals of Zn loaded in compression along directions nearly parallel to the basal planes was due to the operation of  $\langle 11\bar{2}0 \rangle (0001)$  slip, deformation will occur under a falling load and will tend to become localized. Given that the same basal slip is operative in  $\text{Ti}_3\text{SiC}_2$ , this so-called geometric softening is expected and observed.

Because buckling is a result of an instability, it is difficult to model. The difficulty of the task can be appreciated by comparing the micrographs shown in Figures 5(b) and 6(b). Near the center of the micrograph shown in Figure 5(b) and adjacent to the largest delamination flaw, the lower layers of the bent central grain have obviously locally buckled in compression, indicating that, at some point during the deformation, the stress was locally compressive. The same cannot be said about the layers shown in Figure 6(b); the absence of buckling of these very thin lamella precludes compressive stresses.

The deformation of  $\text{Ti}_3\text{SiC}_2$  differs from that of hexagonal metals in one important respect: in metals, clearly identifiable, delaminated lamella are not observed.<sup>[16,17,18]</sup> The propensity for delamination is important in this context because it allows for the very sharp *radii* of curvatures observed. As shown in Figures 6(a) and (b), *radii* of curvatures on the order of  $0.5 \mu\text{m}$  are quite common in  $\text{Ti}_3\text{SiC}_2$  and the  $H$  phases.<sup>[8,9]</sup>

It is important to point out that delamination only occurs when the geometric constraints are relaxed, such as at the corners of the cubes (Figure 4(b)). In the presence of constraints this mode is inoperative, which partially explains why randomly oriented polycrystalline samples fail in a brittle manner. As noted previously, at temperatures higher than  $1200^\circ\text{C}$ , the material exhibits pseudoplasticity or inelastic deformation that is assisted by damage formation in



(a)



(b)

Fig. 6—(a) SEM micrograph of a highly deformed region in  $\text{Ti}_3\text{SiC}_2$ . The sample was hit with a hammer that caused it to fracture along the plane observed. (b) A higher magnification of the prominent feature labeled 'a' in (a).

the form of grain-boundary cracks, kinking, and delamination of individual grains.<sup>[13]</sup> However, in contrast to most lamellar microstructures, the initiation of damage does not result in catastrophic failure because  $\text{Ti}_3\text{SiC}_2$  exhibits an unusual capacity to confine the spatial extent of the damage.<sup>[11,13]</sup> These comments notwithstanding, the plasticity seen in this work is real in the sense that it is dependent on dislocation motion and shear-band formation. The nature of that plasticity, however, does not imply ductile behavior under tensile conditions.

It is well established that microbuckling of fiber bundles accompanied by fiber fracture along a kink boundary is the fundamental damage mechanism under compression in various unidirectional and two-dimensional C-laminated composites.<sup>[31,32,33]</sup> In these systems, delamination is a serious problem. Although individual grains in  $\text{Ti}_3\text{SiC}_2$  have a propensity for delamination, when it occurs, it is noncatastrophic. More importantly, in contrast to kink bands that form in C composites, the lamella in  $\text{Ti}_3\text{SiC}_2$ , for the most part, do not fracture (Figure 6(b)). In that respect, the kink bands in  $\text{Ti}_3\text{SiC}_2$  are similar to those observed in some oriented polymer fibers, where in both cases the lamella or fibrils are continuous across the kink plane.<sup>[23-27]</sup> In one of



Fig. 7—Polished and etched optical micrograph of a near-surface feature of a sample that was deformed to a strain of more than 50 pct.

the earliest studies on kink-band formation in highly oriented nylon, Zaukelies<sup>[25]</sup> sought to explain his results in terms of Orowan's model. Later, Robertson<sup>[23]</sup> showed that kink bands in high-density polyethylene initiate at sites of shear stress concentrations, where the fibrils are first deformed in an S-shaped curve that then tightens and finally collapses into angular kinks. This collapse is much less common in  $\text{Ti}_3\text{SiC}_2$  and appears to occur only when the radii of curvature are very sharp ( $<1 \mu\text{m}$ ). Figure 6(b) is a high-magnification scanning electron microscopy (SEM) micrograph of the prominent feature seen in Figure 6(a), where it is obvious that, while the outer layers are continuous, the innermost layer has obviously collapsed. The resemblance of this micrograph to that of Figure 11 in Reference 23 is striking.

Here again, despite the apparent similarities, important differences, other than the obvious ones relating to the nature of the bonding, morphology, etc., remain. First, delaminations such as those visible in  $\text{Ti}_3\text{SiC}_2$  are usually not observed in oriented polymers. Second, whereas one could possibly make the case that a single grain of  $\text{Ti}_3\text{SiC}_2$  and a highly oriented fiber are similar in their deformation mechanisms, there is no polymer analog to the polycrystalline samples tested here. Third,  $\text{Ti}_3\text{SiC}_2$  involves, as shown in Figure 6(a), the kinking of sheets rather than fibrils. (To produce this micrograph, a sample was hit with a hammer, which caused it to fracture along the plane observed in the micrograph.) This micrograph is reminiscent of what milles feuilles or phyllo dough, before being baked, would appear like under an SEM.

The extent by which a single grain of  $\text{Ti}_3\text{SiC}_2$  can deform, curl, and fold on itself when highly deformed (Figure 7) is unusual. The micrograph shown in Figure 7 is that of a feature observed near the edge of a specimen that was deformed  $\approx 50$  pct. This flexibility, typically absent in other layered compounds such as mica and graphite, can be traced to the metallic nature of the bonding, the absence of strong in-plane Si-Si bonds, and the relative weakness of the Ti-Si bonds.<sup>[9,35,36]</sup>

The technological importance of the results presented here cannot be overemphasized,  $\text{Ti}_3\text{SiC}_2$  is a potentially excellent material for a myriad of high-temperature applica-

tions. The brittle failure of randomly oriented polycrystals at temperatures <1200 °C and the fabrication route described in this article, which would not be suitable for large-scale production, are obvious limitations. Based on this work, the strategy for fabricating ductile samples (at least in compression) would be to align the grains before allowing them to grow. Given the plate-like nature of  $\text{Ti}_3\text{SiC}_2$ , grain alignment using well-established ceramic processing techniques such as slip or tape casting should be straightforward.

#### IV. CONCLUSIONS

Oriented large-grained polycrystalline samples of  $\text{Ti}_3\text{SiC}_2$  are ductile in compression at room temperature. This carbide, and, by extension, other 312 and 211-phases, deforms by a combination of delamination and kink-band formation of individual grains, together with shear-band formation. It is this unique multiplicity of deformation modes that allows the material to deform plastically in any arbitrary orientation.

#### ACKNOWLEDGMENTS

We thank our colleagues Professors A. Zavaliangos, R. Doherty, and S. Kalidindi and Dr. L. Farber for many useful and stimulating discussions. This work was sponsored by the Air Force Office of Scientific Research and the Division of Materials Research, National Science Foundation.

#### REFERENCES

1. W. Jeitschko and H. Nowotny: *Monatsh Chem.*, 1967, vol. 98, pp. 329-37.
2. J.J. Nickl, K.K. Schweitzer, and P. Luxenberg: *J. Less Common Met.*, 1972, vol. 26, p. 283.
3. T. Goto and T. Hirai: *Mater. Res. Bull.*, 1987, vol. 22, pp. 1195-1202.
4. R. Pampuch, J. Lis, L. Stobierski, and M. Tymkiewicz: *J. Eur. Ceram. Soc.*, 1989 vol. 5, p. 283.
5. R. Pampuch, J. Lis, J. Piekarczyk, and L. Stobierski: *J. Mater. Synth. Proc.*, 1993, vol. 1, p. 93.
6. J. Lis, Y. Miyamoto, R. Pampuch, and K. Tanihata: *Mater. Lett.*, 1995, vol. 22, pp. 163-68.
7. M.W. Barsoum and T. El-Raghy: *J. Am. Ceram. Soc.*, 1996, vol. 79, pp. 1953-56.
8. M.W. Barsoum, D. Brodtkin, and T. El-Raghy: *Scripta Metall. Mater.*, 1997, vol. 36, pp. 535-41.
9. M.W. Barsoum and T. El-Raghy: *J. Mater. Synth. Proc.*, 1997, vol. 5, pp. 203-22.
10. M.W. Barsoum, G. Yaroshchuck, and S. Tyagi: *Scripta Mater.*, 1997, vol. 10, pp. 1583-91.
11. T. El-Raghy, A. Zavaliangos, M.W. Barsoum, and S. Kalidindi: *J. Am. Ceram. Soc.*, 1997, vol. 80, pp. 513-16.
12. M.W. Barsoum, T. El-Raghy and L. Ogbuji: *J. Electrochem. Soc.*, 1997, vol. 144, pp. 2508-16.
13. T. El-Raghy, M.W. Barsoum, A. Zavaliangos, and S. Kalidindi: unpublished research, Drexel Univ., Philadelphia, PA, 1998.
14. T. El-Raghy and M.W. Barsoum: unpublished research, Drexel Univ., Philadelphia, PA 1998.
15. L. Farber, M.W. Barsoum, A. Zavaliangos, T. El-Raghy, and I. Levin: *J. Am. Ceram. Soc.*, 1998, vol. 81, pp. 1677-81.
16. E. Orowan: *Nature*, 1942, vol. 149, pp. 463-64.
17. J.B. Hess and C.S. Barrett: *Trans. AIME*, 1949, vol. 185, p. 599.
18. E.G. Tapetado and M.H. Loretto: *Phil. Mag.*, 1974, vol. 30, p. 515.
19. M.S. Patterson and L.E. Weiss: *Geol. Soc. Am. Bull.*, 1996, vol. 77, pp. 343-73.
20. O. Mugge: *Neues Jarrb. Miner.*, 1898, vol. 1, p. 71.
21. N.C. Gay and L.E. Weiss: *Tectonophysics*, 1974, vol. 21, p. 287.
22. E. Honea and A.M. Johnson: *Tectonophysics*, 1976, vol. 30, p. 197.
23. R.E. Robertson: *J. Polymer Sci.*, 1980, vol. A-27, pp. 1315-28.
24. S. DeTeresa, R. Porter, and R. Farris: *J. Mater. Sci.*, 1988, vol. 23, pp. 1886-94.
25. D.A. Zaukelies: *J. Appl. Phys.*, 1962, vol. 33, pp. 2797-2803.
26. G.E. Attenburrow and D.C. Bassett: *J. Mater. Sci.*, 1979, vol. 14, pp. 2679-87.
27. A. Keller and J.G. Rider: *J. Mater. Sci.*, 1966, vol. 1, p. 389.
28. C.T. Keith and W.A. Cote, Jr.: *Forest Prod. J.*, 1968, vol. 18, p. 67.
29. H.M. Hathorne and E. Teghtsoonian: *J. Mater. Sci.*, 1975, vol. 10, pp. 41-51.
30. W.R. Jones and J.W. Johnson: *Carbon*, 1971, vol. 9, p. 645.
31. V. Gupta, K. Anand, and M. Kryska: *Acta Metall. Mater.*, 1994, vol. 42, pp. 781-95.
32. C.W. Weaver and J.G. Williams: *J. Mater. Sci.*, 1975, vol. 10, pp. 1323-33.
33. A.S. Argon: *Treatise Mater. Sci. Technol.*, 1972, vol. 1, p. 79.
34. G.R. Edwards, J. Shyne, and O. Sherby: *Metall. Trans.*, 1971, vol. 2, pp. 2955-58.
35. M. Amer, M.W. Barsoum, T. El-Raghy, I. Wiess, S. LeClair, and D. Liptak: *J. Appl. Phys.*, in press.
36. M.W. Barsoum, T. El-Raghy, C.J. Rawn, W.D. Porter, H. Wang, E.A. Payzant, and C.R. Hubbard: *J. Phys. Chem. Sol.*, in press.

# Contact Damage Accumulation in $\text{Ti}_3\text{SiC}_2$

It Meng Low,<sup>†</sup> Seung Kun Lee,<sup>\*‡</sup> and Brian R. Lawn<sup>\*</sup>

Materials Science and Engineering Laboratory, National Institute of Standards and Technology,  
Gaithersburg, Maryland 20899

Michel W. Barsoum<sup>\*</sup>

Department of Materials Engineering, Drexel University, Philadelphia, Pennsylvania 19104

The evolution of deformation-microfracture damage below Hertzian contacts in a coarse-grain  $\text{Ti}_3\text{SiC}_2$  is studied. The Hertzian indentation stress-strain response deviates strongly from linearity beyond a well-defined maximum, with pronounced strain-softening, indicating exceptional deformability in this otherwise (elastically) stiff ceramic. Surface and subsurface ceramographic observations reveal extensive quasi-plastic microdamage zones at the contact sites. These damage zones are made up of multiple intra-grain slip and intergrain shear failures, with attendant microfracture at high strains. No ring cracks or other macroscopic cracks are observed on or below the indented surfaces. The results suggest that  $\text{Ti}_3\text{SiC}_2$  may be ideally suited to contact applications where high strains and energy absorption prior to failure are required.

## I. Introduction

RECENTLY, dense polycrystalline  $\text{Ti}_3\text{SiC}_2$  has been developed by reactively hot-pressing Ti, SiC, and C (graphite) powders.<sup>1</sup>  $\text{Ti}_3\text{SiC}_2$  has a hexagonal crystallographic structure with planar Si layers linked by TiC octahedra, and with weakly bonded basal slip planes.<sup>2</sup> This material displays a unique combination of properties.<sup>3</sup> It is oxidation resistant, and possesses high electrical and thermal conductivity. It has a high elastic modulus ( $E \approx 320$  GPa) but a low hardness ( $H \approx 4$  GPa), and is machinable. The value  $H/E = 0.013$  is exceptionally small for a ceramic,<sup>4</sup> more reminiscent of soft metals. In Vickers indentation tests a multiplicity of energy-absorbing deformation mechanisms operate, predominantly basal slip but also grain buckling as well as grain sliding.<sup>3</sup>

In this communication we investigate the contact deformation of  $\text{Ti}_3\text{SiC}_2$  using Hertzian indentation.<sup>5,6</sup> Indentation stress-strain data reveal exceptional quasi-plasticity in this material, with a pronounced strain-softening "tail." Ceramographic sectioning is used to examine the nature of the subsurface quasi-plastic damage. Our experiments confirm shear-activated basal slip deformation within grains as the key to the exceptional high quasi-plasticity.

## II. Experimental Procedure

Details to the powder processing and ensuing microstructure of  $\text{Ti}_3\text{SiC}_2$  have been presented elsewhere.<sup>1</sup> Polycrystalline

specimens were fabricated by weighing stoichiometric proportions of Ti (99.3% pure, 325 mesh, Titanium Specialists, Sandy, UT), SiC (99.7% pure, mean particle size 4  $\mu\text{m}$ , Atlantic Equipment Engineers, Bergenfield, NJ), and C (99% pure, mean particle size 1  $\mu\text{m}$ , Aldrich, Milwaukee, WI) powders, mixing in a V-blender for 2 h, and reactive hot pressing at 1600°C for 4 h under a pressure of 40 MPa. The microstructure of the sintered material investigated here consists of large platelike grains of diameter 50–200  $\mu\text{m}$  and thickness 5–20  $\mu\text{m}$ , with a heavily striated texture.<sup>1,3</sup> All test surfaces were diamond-polished to 1  $\mu\text{m}$  finish.

Vickers indentations were made at  $P = 1$ –1000 N to measure hardness, determined here as  $H = P/2a^2$ , where  $P$  is peak load and  $a$  is impression half-diagonal.

Hertzian indentations were made using tungsten carbide (WC) spheres of radius  $r = 1.21$ –12.7 mm, at peak loads up to  $P = 4000$  N. Measurements of contact radius  $a$  (made visible by first coating the specimen surface with a gold film) at each given load  $P$  and sphere radius  $r$  enabled calculation of indentation stresses,  $p_0 = P/\pi a^2$ , and indentation strains,  $a/r$ , for construction of an indentation stress-strain curve.<sup>5,7</sup> An indentation yield stress  $p_0 = p_Y$  was evaluated from the threshold loads above which permanent impressions were first detected on the contact surface.<sup>8</sup>

Bonded-interface specimens were used to provide sections of the Hertzian contact damage.<sup>5,7</sup> These specimens were prepared by bonding together two polished half-blocks 30 mm  $\times$

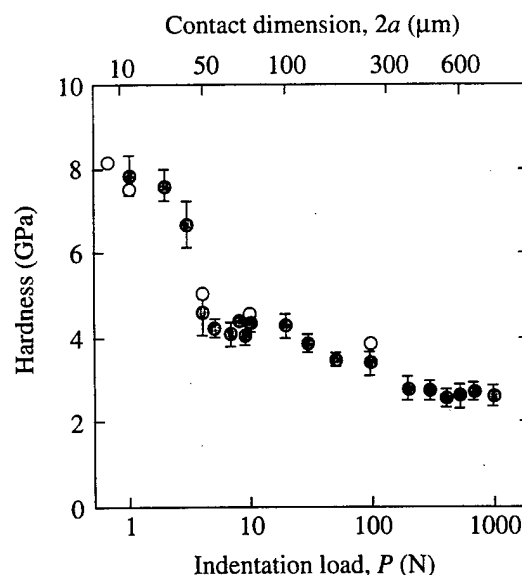


Fig. 1. Vickers hardness (means and standard deviations) as function of indentation load for  $\text{Ti}_3\text{SiC}_2$ . Open circles are data from previous work.<sup>3</sup>

J. E. Ritter—contributing editor

Manuscript No. 190643. Received October 6, 1997; approved November 19, 1997. Supported by the U.S. Air Force Office of Scientific Research.

<sup>\*</sup>Member, American Ceramic Society.

<sup>†</sup>Guest Scientist from the Department of Applied Physics, Curtin University of Technology, Perth WA 6001, Australia.

<sup>‡</sup>Guest Scientist from the Department of Materials Science and Engineering, Lehigh University, Bethlehem, Pennsylvania 18015.

10 mm  $\times$  10 mm at a common interface with an intervening thin layer of adhesive, and then polishing the top surface. Indentations were made on the top surface across the surface trace of the bonded interface. The adhesive was then dissolved in acetone, and the top and side surfaces of the separated half-blocks gold coated. Damage zones were observed by optical microscopy in Nomarski illumination and by scanning electron microscopy (SEM).

### III. Results

#### (1) Hardness and Indentation Stress-Strain Curve

Figure 1 plots hardness as a function of indentation load for the  $\text{Ti}_3\text{SiC}_2$  material. Each data point (mean and standard deviation) was obtained from five measurements. Some data from previous work on similar material are included for comparison.<sup>3</sup> The hardness is highly dependent on the indentation load, falling first abruptly between  $P = 1\text{--}5\text{ N}$  and then more gradually at higher loads. This strong dependency of hardness is attributable to the large grain size: when the contact dimension  $2a$  of the Vickers impression is less than the grain size (minimum  $50\text{ }\mu\text{m}$ ), the hardness measures properties of single grains; when  $2a$  becomes much larger than the grain size, the hardness measures polycrystalline properties, with more grains oriented for basal slip. The relatively large error bars associated with the data at low loads in Fig. 1 reflect stochastic in the grain orientations in this region.<sup>5</sup>

Figure 2 plots the Hertzian indentation stress-strain curve. The data points are experimental values for the different sphere

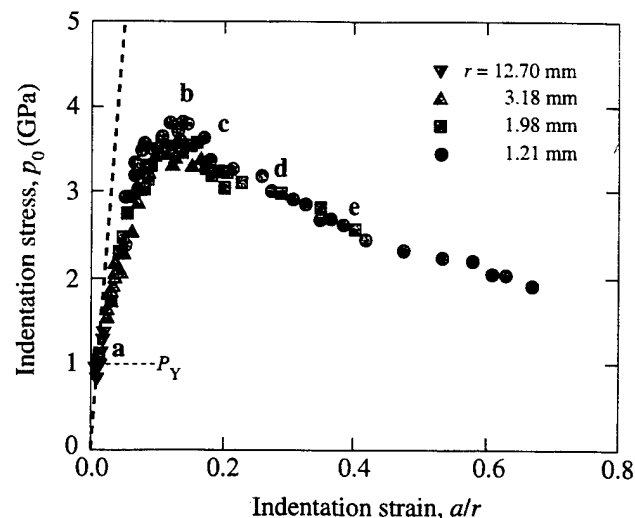


Fig. 2. Indentation stress-strain curve for  $\text{Ti}_3\text{SiC}_2$ . Inclined dashed line is Hertzian elastic response. Labels a, b, c, d, and e correspond to micrographs in Fig. 3.

sizes. The inclined dashed line through the origin is the Hertzian limit for ideal elastic contacts. A yield point  $p_Y = 1.0\text{ GPa}$  representing the contact pressure at first observable deformation is indicated. The data deviate slightly from linearity above this yield point, increasing monotonically with load.<sup>5,6,9</sup>

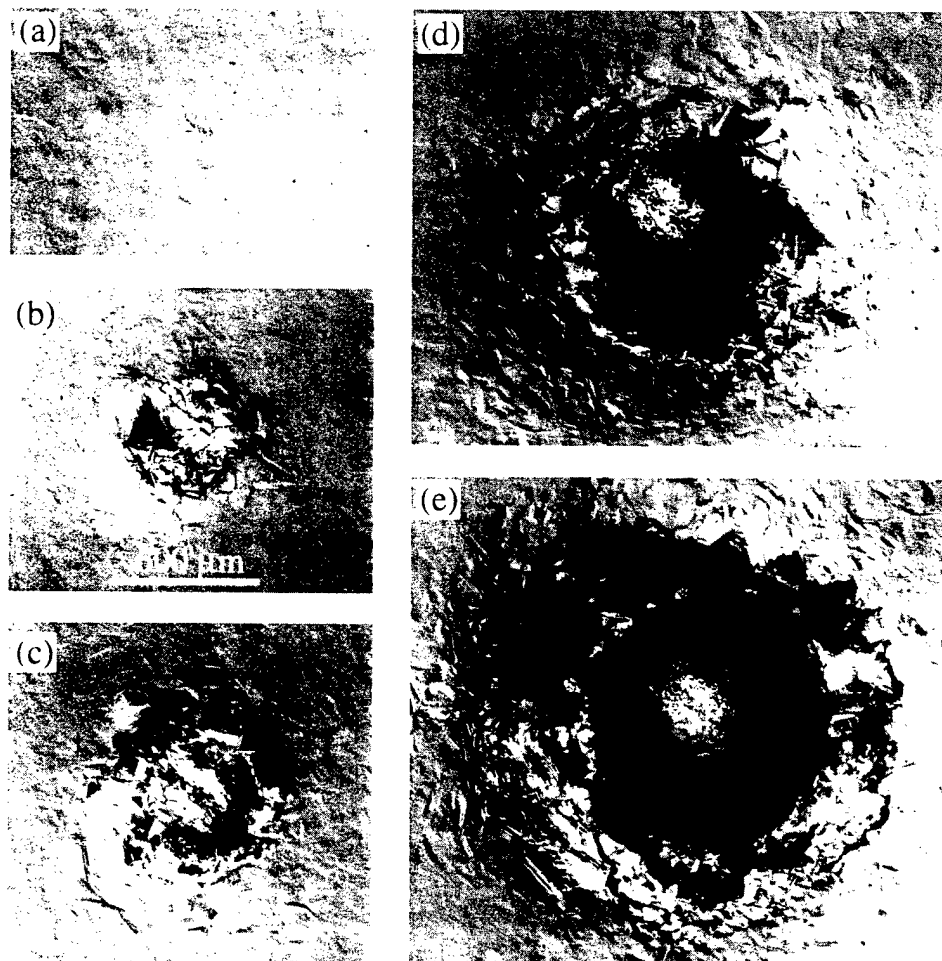


Fig. 3. Surface views of indentation sites in  $\text{Ti}_3\text{SiC}_2$ . Indentations made with WC ball of radius  $r = 1.98\text{ mm}$ . Micrographs (a), (b), (c), (d), and (e) correspond to points labeled in Fig. 2. Optical micrographs, Nomarski illumination.

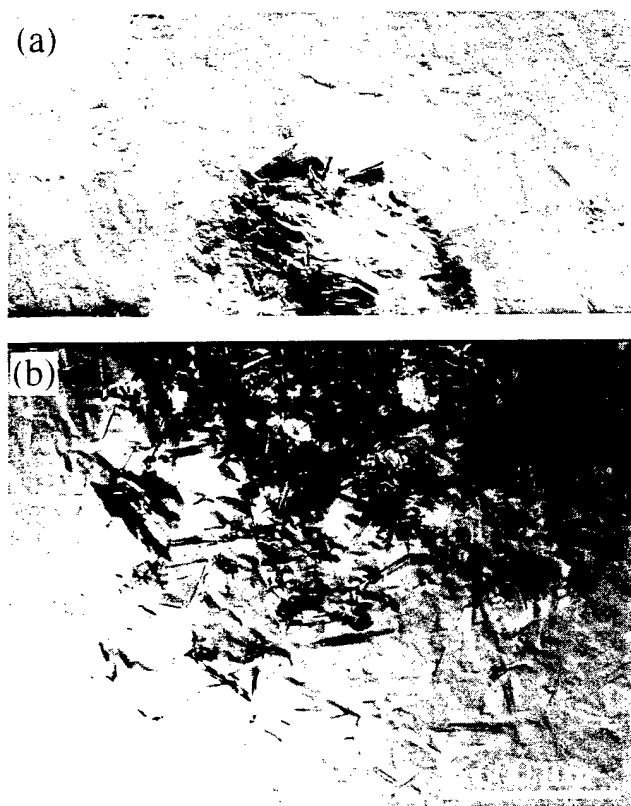


Fig. 4. Half-surface and side view of contact damage from WC ball radius  $r = 3.18$  mm at load  $P = 2000$  N ( $p_0 = 3.6$  GPa). Bonded-interface specimen.

However, the data then pass through a distinctive maximum at  $p_0 \approx 3.8$  GPa and thereafter decline steadily in a long tail. This kind of strong strain-softening characteristic is most unusual in ordinarily brittle ceramics, although it is reminiscent of the stress-strain curves observed in rocks in triaxial compression fields.<sup>10</sup>

## (2) Contact Damage and Deformation

The optical micrographs in Fig. 3 confirm that the deviation from linearity in the stress-strain curve is due to the onset of indentation damage. The sequence shows surface views of damage for points marked **a**, **b**, **c**, **d**, and **e** in Fig. 2: (a) just above the yield point the first few grains have deformed within the contact area; (b) near the maximum the number of deformed grains within the contact area has markedly increased and individual grain-localized microfaults are observed, typical of tough ceramics;<sup>5,6,9</sup> (c) beyond the maximum stress level the impression is more extensive and deformed grains are observed outside the impression; (d) further along the strain-softening tail the impression is deeper and grain deformation outside the contact area is considerably more pronounced, and material has piled up around the impression; (e) at even higher strain the impression is extensive, and grains beyond the edge of the contact area are heavily deformed, with attendant microcrack coalescence and grain detachment. The complete absence of any ring cracks or cone cracks on the surfaces highlights the predominantly quasi-plastic nature of the damage.

Figure 4 shows a half-surface and section view of the contact damage near the stress-strain maximum (just beyond point **b** in Fig. 2). A distinctive surface depression is observed in the section, attesting to the extent of the deformation. The subsurface deformation is particularly intense, extending well below the contact area. Figure 5 shows optical and SEM micrographs of the center region of the subsurface damage zone in Fig. 4(b). In Fig. 5(a) intralamella slip along basal planes and microfailures along the grain boundaries are evident. In Fig. 5(b) mi-

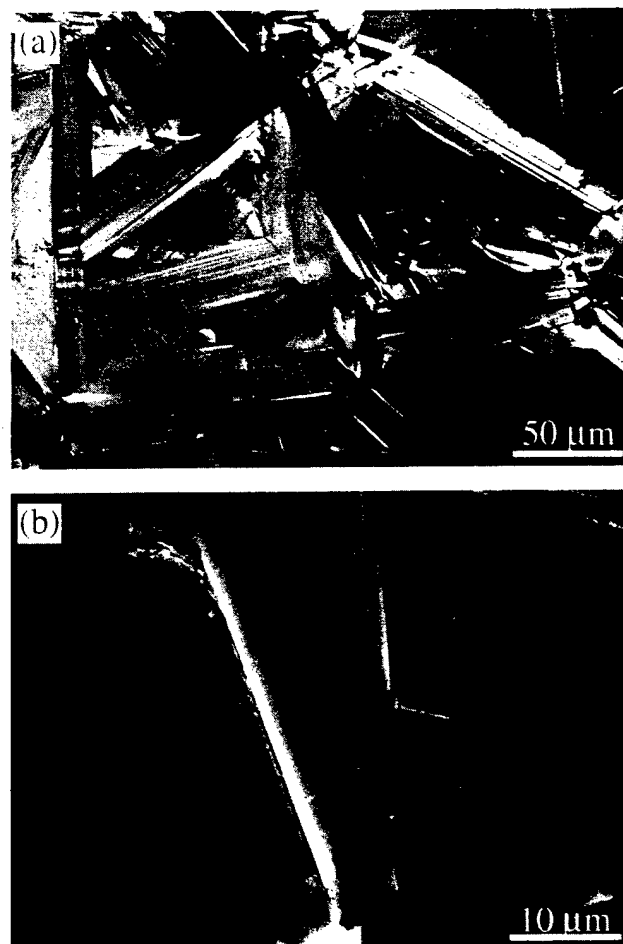


Fig. 5. Micrographs of micromechanical damage from central subsurface region in Fig. 4: (a) optical (Nomarski), (b) SEM.

crofailures extend along the grain boundaries intersected by the heavily deformed lamellae, analogous to the generation of microcracks at dislocation pile-ups in metals,<sup>11</sup> and across some of the adjacent grains.

## IV. Discussion

We have investigated contact damage in  $\text{Ti}_3\text{SiC}_2$  using Hertzian contact. The indentation stress-strain curve in Fig. 2 reveals some distinctive features in the elastic-plastic response. The initial elastic region is steep, commensurate with the high Young's modulus, 320 GPa (a value comparable to that of other hard ceramics like silicon nitride and alumina). The stress-strain curve deviates slightly from linearity above the yield stress,  $p_Y = 1.0$  GPa, up to the maximum,  $p_0 = 3.8$  GPa. Beyond this point the curve decreases dramatically with increasing strain, indicating strong strain-softening. Such softening behavior is most unusual in ordinarily brittle ceramics (although it is observed commonly in rocks in compression<sup>10</sup>), reflecting the capacity of the material to undergo extensive plastic deformation without macroscopic fracture. The low ratio of hardness/modulus,  $H/E = 0.013$ , is comparable to soft steel,<sup>4</sup> suggesting an ultimate mechanical behavior more reminiscent of a ductile metal.

There is a microstructural size effect in the Vickers hardness data in Fig. 1.<sup>3</sup> This size effect is associated with the large grain size of the  $\text{Ti}_3\text{SiC}_2$  material studied here. When the contact area is comparable to the grain size, the contact samples just a few grains—the probability of initiating slip then depends strongly on the local grain orientation. As the contact area increases, more grains are sampled within the near-contact field, and the

likelihood of encountering grains with favorable orientations for deformation is correspondingly higher. Accordingly, the data are subject to greater stochastic variation at low loads,<sup>5</sup> accounting for the larger error bars in this region in Fig. 1.

The micrographs of the damage zones in Figs. 3 and 4 demonstrate extensive shear-driven deformation in the  $\text{Ti}_3\text{SiC}_2$ . The high-magnification micrographs in Fig. 5 reveal the damage to consist predominantly of basal-slip lamellae within grains, with accompanying shear-induced microcracking between grains. The ease and multiplicity of the basal slip process within the individual grains accounts for the exceptional plasticity.<sup>1,3,12</sup> On the other hand, the existence of just one easy slip system precludes a totally plastic response, and ultimately the local strains at the grain boundaries can only be accommodated by the generation of intergranular (or intragranular<sup>3</sup>) microcracks. As these microcracks multiply, extend, and (ultimately) coalesce the modulus of material within the damage zone correspondingly diminishes,<sup>13,14</sup> accounting for the strain-softening seen in Fig. 2.<sup>10</sup> In combination, these easy deformation and microfracture processes at the microstructural level render the material machinable.<sup>1</sup> Other machinable ceramics with platelet structures, e.g., micaceous glass-ceramics ("Macor"),<sup>15</sup> show analogous easy lamella slip, but not to the degree observed in the present material, and without the distinctive strain-softening in the indentation stress-strain curve.<sup>7</sup> The indications are that the present material is somewhat more plastic than the micaceous glass-ceramics, but at the same time still somewhat more brittle than metals with multiple slip systems.

The extreme plasticity of  $\text{Ti}_3\text{SiC}_2$  lends itself to applications in which high energy absorption with attendant high strains to failure, without microscopic cracking, are a prime requisite. In this sense,  $\text{Ti}_3\text{SiC}_2$  has the mechanical quality of metals, but still with high elastic rigidity and high-temperature properties characteristic of ceramics. On the other hand, the proliferation of microcracking associated with the quasi-plasticity damage foreshadows some potential limitations, e.g., susceptibility to fatigue<sup>16,17</sup> and low wear resistance.<sup>18</sup>

**Acknowledgments:** We are grateful to T. El-Raghy for supplying us with specimens for this work. We also wish to thank I. M. Peterson, S. Wut-

tiphan, Y. G. Jung, and H. Chai for many discussions on experimental aspects of this work.

## References

- <sup>1</sup>M. W. Barsoum and T. El-Raghy, "Synthesis and Characterization of a Remarkable Ceramic:  $\text{Ti}_3\text{SiC}_2$ ," *J. Am. Ceram. Soc.*, **79** [7] 1953-56 (1996).
- <sup>2</sup>W. Jeitschko and H. Nowotny, "Die Kristallstruktur von  $\text{Ti}_3\text{SiC}_2$ —Ein Neuer Komplexcarbidge-Typ," *Monatsh. Chem.*, **98**, 329-37 (1967).
- <sup>3</sup>T. El-Raghy, A. Zavaliangos, M. W. Barsoum, and S. R. Kalidindi, "Damage Mechanisms around Hardness Indentations in  $\text{Ti}_3\text{SiC}_2$ ," *J. Am. Ceram. Soc.*, **80** [2] 513-16 (1997).
- <sup>4</sup>B. R. Lawn and V. R. Howes, "Elastic Recovery at Hardness Indentations," *J. Mater. Sci.*, **16**, 2745-52 (1981).
- <sup>5</sup>F. Guiberteau, N. P. Padture, and B. R. Lawn, "Effect of Grain Size on Hertzian Contact Damage in Alumina," *J. Am. Ceram. Soc.*, **77** [7] 1825-31 (1994).
- <sup>6</sup>S. K. Lee, S. Wuttiphan, and B. R. Lawn, "Role of Microstructure in Hertzian Contact Damage in Silicon Nitride: I. Mechanical Characterization," *J. Am. Ceram. Soc.*, **80** [9] 2367-81 (1997).
- <sup>7</sup>H. Cai, M. A. Stevens Kalceff, and B. R. Lawn, "Deformation and Fracture of Mica-Containing Glass—Ceramics in Hertzian Contacts," *J. Mater. Res.*, **9** [3] 762-70 (1994).
- <sup>8</sup>R. M. Davies, "Determination of Static and Dynamic Yield Stresses Using a Steel Ball," *Proc. R. Soc. London*, **A197** [1050] 416-32 (1949).
- <sup>9</sup>B. R. Lawn, N. P. Padture, H. Cai, and F. Guiberteau, "Making Ceramics 'Ductile,'" *Science*, **263**, 1114-16 (1994).
- <sup>10</sup>J. C. Jaeger and N. G. W. Cook, *Fundamentals of Rock Mechanics*; Ch. 4. Chapman and Hall, London, U.K., 1971.
- <sup>11</sup>B. R. Lawn, *Fracture of Brittle Solids*; Ch. 9. Cambridge University Press, Cambridge, U.K., 1993.
- <sup>12</sup>B. R. Lawn and D. B. Marshall, "Nonlinear Stress-Strain Curves for Solids Containing Closed Cracks with Friction," *J. Mech. Phys. Solids*, in press.
- <sup>13</sup>J. B. Walsh, "The Effect of Cracks on the Uniaxial Elastic Compression of Rocks," *J. Geophys. Res.*, **70** [2] 399-411 (1965).
- <sup>14</sup>B. R. Lawn, S. K. Lee, I. M. Peterson, and S. Wuttiphan, "A Model of Strength Degradation from Hertzian Contact Damage in Tough Ceramics," *J. Am. Ceram. Soc.*, in press.
- <sup>15</sup>K. Chyung, G. H. Beall, and D. G. Grossman, "Fluorophlogopite Mica Glass-Ceramics," pp. 33-40 in Proceedings of the 10th International Glass Congress, No. 14, Edited by M. Kunugi, M. Tashiro, and N. Saga. Ceramic Society of Japan, Kyoto, Tokyo, Japan, 1974.
- <sup>16</sup>H. Cai, M. A. S. Kalceff, B. M. Hooks, B. R. Lawn, and K. Chyung, "Cyclic Fatigue of a Mica-Containing Glass-Ceramic at Hertzian Contacts," *J. Mater. Res.*, **9** [10] 2654-61 (1994).
- <sup>17</sup>N. P. Padture and B. R. Lawn, "Contact Fatigue of a Silicon Carbide with a Heterogeneous Grain Structure," *J. Am. Ceram. Soc.*, **78** [6] 1431-38 (1995).
- <sup>18</sup>V. S. Nagarajan and S. Jahanmir, "The Relationship between Microstructure and Wear of Mica-Containing Glass-Ceramics," *Wear*, **200**, 176-85 (1996). □

# Dislocations and Stacking Faults in $\text{Ti}_3\text{SiC}_2$

Leonid Farber, Michel W. Barsoum,\* Antonios Zavaliangos, and Tamer El-Raghy

Department of Materials Engineering, Drexel University, Philadelphia, Pennsylvania 19104

Igor Levin\*

Ceramics Division, National Institute of Standards and Technology, Gaithersburg, Maryland 20899-0001

The ternary carbide  $\text{Ti}_3\text{SiC}_2$  fabricated by a reactive hot-press route is investigated by transmission electron microscopy. The material consists mainly of large elongated grains with planar boundaries, and is characterized by a low defect density. Dislocations are observed in the grains and at grain boundaries. Perfect dislocations with  $b = \frac{1}{3}\langle 11\bar{2}0 \rangle$  lying in (0001) basal planes are present. These basal plane dislocations are mobile and multiply as a result of room-temperature deformation. All of the stacking faults observed lie in the basal planes.

## I. Introduction

RECENTLY, we reported on the fabrication and characterization of the layered ternary compound  $\text{Ti}_3\text{SiC}_2$ .<sup>1-5</sup> This compound was found to combine many of the best attributes of metals and ceramics. Like metals, it is an excellent electric and thermal conductor, very readily machinable, relatively soft (with a hardness of 4 GPa) compared to other carbides, and is highly thermal shock resistant. Above 1200°C the material exhibits significant ductility. At 1300°C, its yield stress is 100 and 500 MPa in flexure and compression, respectively. Like ceramics it is elastically rigid with a Young modulus of 320 GPa, oxidation and creep resistant,<sup>3</sup> and stable to at least 1700°C in inert atmospheres and under vacuum.<sup>2</sup>

More recently, we have shown that oriented coarse-grained (1–3 mm) polycrystalline samples of  $\text{Ti}_3\text{SiC}_2$  loaded in compression at room temperature deformed plastically.<sup>5</sup> When the basal planes were oriented favorably to the applied stress, substantial (>20%) deformation occurred by the formation of shear bands along those planes, implying that the main deformation mechanism was basal slip. The results reported herein confirm this conclusion. Furthermore, when the slip planes were parallel to the applied load—a situation where ordinary glide was impossible—deformation occurred by a combination of delamination of individual grains, and the formation of kink and shear bands.

Currently very limited information exists on the structural defects in this material, and thus the exact details of the deformation mechanisms that are operative are totally unknown. To the best of our knowledge, the only other previous papers that dealt with the transmission electron microscopy (TEM) of  $\text{Ti}_3\text{SiC}_2$  are those of Arunajatesan and Carim<sup>6</sup> and Morgiel *et al.*<sup>7</sup> The former, using convergent beam electron diffraction studies, confirmed that the unit cell was indeed hexagonal with lattice parameters  $a = 3.07 \text{ \AA}$  and  $c = 17.69 \text{ \AA}$ , consistent

with previously determined values.<sup>8-10</sup> Morgiel *et al.* hot-pressed polycrystalline bulk samples from powders that were produced by self-propagating high-temperature synthesis. Their material, however, was not single phase, and the focus of their investigation was the identification and characterization of the various phases present by TEM.<sup>7</sup> The authors, however, reported a high density of basal plane dislocations grouped in arrays that ran across grain lengths.

The goal of this work is to characterize by TEM some of the linear and planar defects present in single-phase, bulk, dense samples of  $\text{Ti}_3\text{SiC}_2$  before and after room-temperature deformation.

## II. Experimental Procedure

The fabrication procedure for the material has been described in detail elsewhere.<sup>1,2,5</sup> In short, titanium (99.3%, –325 mesh, Titanium Specialists, Sandy, UT), SiC (99.7%,  $d_m = 4 \text{ \mu m}$ , Atlantic Equipment Engineers, Bergenfield, NJ), and C powders (99%,  $d_m = 1 \text{ \mu m}$ , Aldrich) were weighed and dry mixed in a V-blender (Patterson-Kelly Co., East Stroudsburg, PA) for 2 h to yield the  $\text{Ti}_3\text{SiC}_2$  stoichiometry. Polycrystalline samples with randomly oriented grains were produced by reactive hot pressing of Ti, SiC, and graphite powders at 1600°C for 4 h. Oriented coarse-grained (2–3 mm) polycrystalline samples were fabricated via a hot forging operation in a channel die, followed by a 1600°C, 24 h anneal during which the grains, which were oriented during the forging operation, grew significantly.<sup>5</sup>

Small cubes were machined and deformed under compression at room temperature as a function of orientation. The details on the mechanical testing are given in Ref. 5. Clear, unambiguous evidence for shear band formation parallel to the basal planes was observed in the oriented coarse-grained samples by optical microscopy. For TEM characterization of the deformed material, sections were taken from an area in the vicinity of the shear bands.

Thin foils for TEM were prepared by slicing 200  $\text{\mu m}$  thick sections from bulk material, followed by thinning and polishing by the Gatan Dimple Grinder (Model 656) and ion milling at 5 kV/20 mA by the Gatan Precision Ion Polishing System (Model 691). Microstructure observation was performed in JEOL 100CX2 and Philips 430 transmission electron microscopes at 100 and 300 kV, respectively.

## III. Results

### (1) Undeformed Samples

Scanning electron microscopy (SEM) of the as-fabricated material has shown that the hot-pressed material is composed of elongated grains 100–300  $\text{\mu m}$  long with planar boundaries.<sup>1,2</sup> The hot-forged and annealed material, on the other hand, has an oriented coarse-grained (2–3 mm) microstructure.<sup>5</sup> The material is single phase; no inclusions or other phases are detected in the TEM. A few isolated pores of about

A. H. Carim—contributing editor

Manuscript No. 190632. Received October 16, 1997; approved March 17, 1998.  
Support for L. Farber was provided by the Stein Foundation. Additional support for this work was provided by the Air Force Office of Scientific Research.  
\*Member, American Ceramic Society.

0.1  $\mu\text{m}$  diameter are observed in the material. Analysis of convergent beam and selected area electron diffraction patterns confirmed that the material has a hexagonal structure with lattice parameters  $a = 0.307 \text{ nm}$  and  $c = 1.767 \text{ nm}$ , which is in good agreement with our X-ray diffraction data, as well as with data reported by others.<sup>6,8-10</sup>

Observation of thin foils fabricated from either the 100–300  $\mu\text{m}$  polycrystalline samples or the oriented, but undeformed, coarse-grained samples revealed that the defects in both types of specimens are similar. Some grains are defect free, whereas others contain dislocations, planar defects, or both (Figs. 1–3). The dislocations can be categorized according to their arrangement within the grain and association with other dislocations and planar defects. The following dislocations are observed: single dislocations (A in Fig. 1(a)), arrays of parallel straight and curved dislocations within a grain (B in Figs. 1(a) and (b)), dislocations bounding planar defects (C in Figs. 2(c) and (d)), and dislocations at grain boundaries (D in Fig. 1(a)).

Single dislocations (A in Fig. 1) are scarce; only a few of them are observed in some grains. These dislocations tend to be close to the grain boundaries and are usually straight and lie in the basal planes. Arrays of parallel dislocations are observed near some triple junctions and grain boundaries (B in Figs. 1(a) and (b)) and crack tips (B in Fig. 3(a)). These cracks (not shown in Fig. 3) are believed to have formed during specimen preparation. It is important to point out that in contrast to the arrays observed after deformation, the extent and number of the arrays is quite limited before deformation. For example, when observed at all, the arrays rarely extend more than 2–3  $\mu\text{m}$ , i.e., 5–15 dislocations into the grain interior (Fig. 1(b)). Tilting experiments revealed that the randomly distributed isolated dislocations and arrays of parallel dislocations like those shown in Fig. 1 are invisible when imaged with  $g = 1\bar{1}00$  and  $1\bar{1}02$ , but visible when imaged with complementary  $0\bar{1}10$  and  $10\bar{1}0$  reflections, as well as with all three  $11\bar{2}0$  type reflections. Consequently, these dislocations are perfect with a Burgers vector of the  $\frac{1}{3}\langle 11\bar{2}0 \rangle$  type, and all lie in the basal plane. It is worth noting that while the vast majority of dislocations were basal plane dislocations, in a few isolated cases, they did not appear to lie totally in the basal planes; the nature of these dislocations is still unclear at this time.

Numerous planar defects are also observed. They can be divided into two types, depending on their extent. Defects of the first type extend clear across the grains. Typically, one or two such defects are observed per grain. In Figs. 2(a) and (b), such a defect, labeled SF, propagates across the grain G2. Selected area diffraction patterns for regions on both sides of the defect are identical, confirming that G2 constitutes a single grain containing this planar defect. Furthermore, the contrast associated with the defect as well as its absence is easily observed by tilting the specimens and imaging the defects with various reflections. As shown in Figs. 2(a) and (b), the defect is invisible when imaged with  $g = 1\bar{2}10$  but is visible with  $g = 0\bar{1}14$ . In the latter case, alternating bright and dark fringes are observed, which are of symmetrical contrast in bright field and asymmetrical contrast in dark field (not shown). Thus, the defect must be stacking fault characterized by a displacement vector parallel to  $[0001]$ .

Defects of the second kind are similar to the first, except that they do not propagate across the whole grain (Figs. 2(c) and (d) and C in Figs. 3(a) and (b)). Such faults are usually grouped in bands extending from the grain boundaries and bounded by partial dislocations lying inside the grain. Contrast analysis revealed that the faults and their bounding dislocations (C in Fig. 3) became invisible when imaged with  $g = 11\bar{2}0$  type and visible with  $g = 0002$  type as shown in Fig. 3, which shows a typical example of a grain with the basal planes in an edge-on position. In this figure, C points to partial dislocations bounding the stacking faults which propagate from the upper left corner of the figure that were similar to those shown in Figs. 2(c, d). These defects and the partials are visible as a line when imaged with  $g = 0002$ . But, as shown in Fig. 3(b), the stacking faults and their bounding dislocations become invisible when imaged with  $g = 11\bar{2}0$ , which strongly suggests that the stacking faults are characterized by a displacement vector parallel to  $[0001]$ . All of the planar defects observed in this work and their bounding dislocations lie in the basal plane.

Most grain boundaries contain dislocations. In some cases, faceting of grain boundaries has also been observed. Pores were scarce and typically had a shape reminiscent of a parallelepiped, i.e., were apparently bounded by low index planes, presumably basal and prismatic ones.

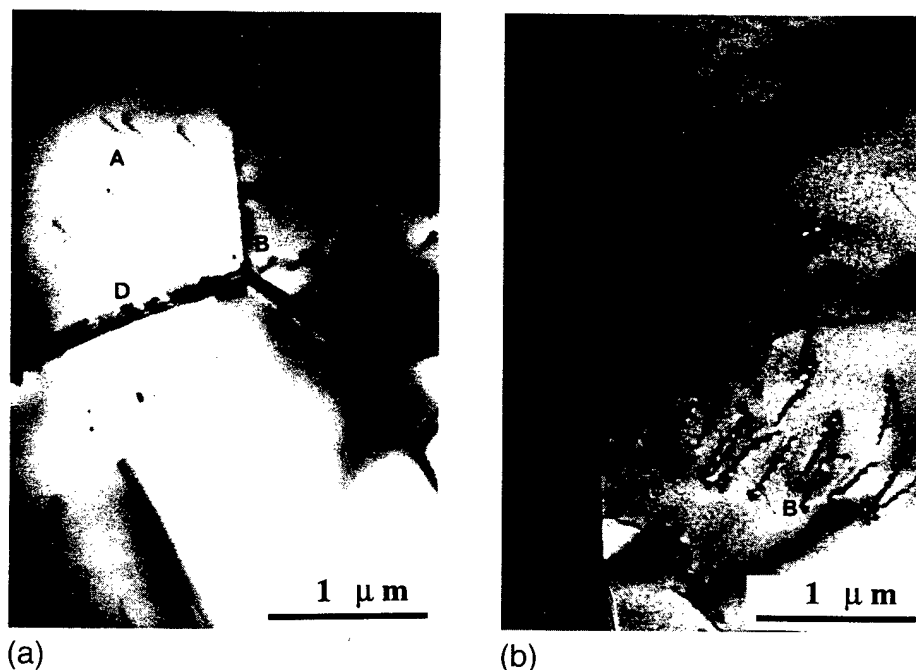
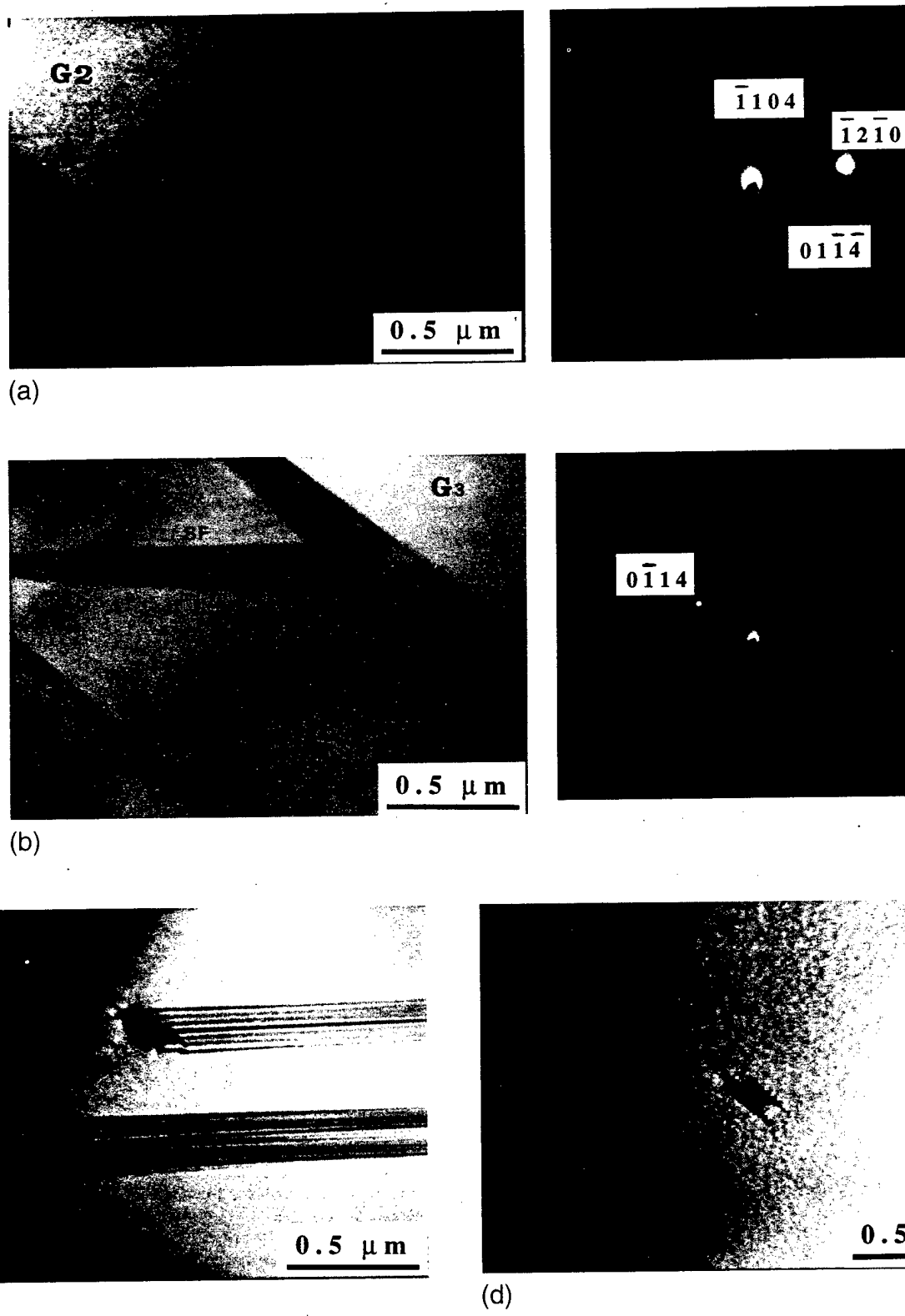


Fig. 1. Typical dislocations in  $\text{Ti}_3\text{SiC}_2$  produced by reactive hot pressing: single dislocations (A); arrays of parallel straight dislocations within a grain (B); dislocations bounding stacking faults (C); dislocations at grain boundaries (D).



**Fig. 2.** (a) Single stacking fault, SF, propagating across grain  $G_2$ . Grains  $G_1$  and  $G_3$  are two adjacent grains separated from  $G_2$  by boundaries  $GB_1$  and  $GB_2$ . Bright field, BF, with  $g = \bar{1}2\bar{1}0$ . (b) BF with  $g = 0\bar{1}14$ . (c) Typical example of second type of stacking faults, in which one side is bounded by partial dislocations and the other (not shown) a grain boundary. (d) Same area as (c), but imaged such that only the bounding dislocations are visible.

## (2) Deformed Samples

In contrast to the low dislocation density in the undeformed material, the dislocation density in the deformed material was significantly higher, as shown in Fig. 4. Tilting experiments revealed that the vast majority of these dislocations lie in the basal planes. The dislocations are grouped in basal plane arrays

that propagate through the whole transparent field of view. Within an array, the dislocations are parallel and equidistant, suggesting that they all propagate along the same slip plane. The number and spatial extent of the arrays are significantly enhanced as a result of the deformation. We did not observe any dislocation entanglements or evidence for cross-slip.

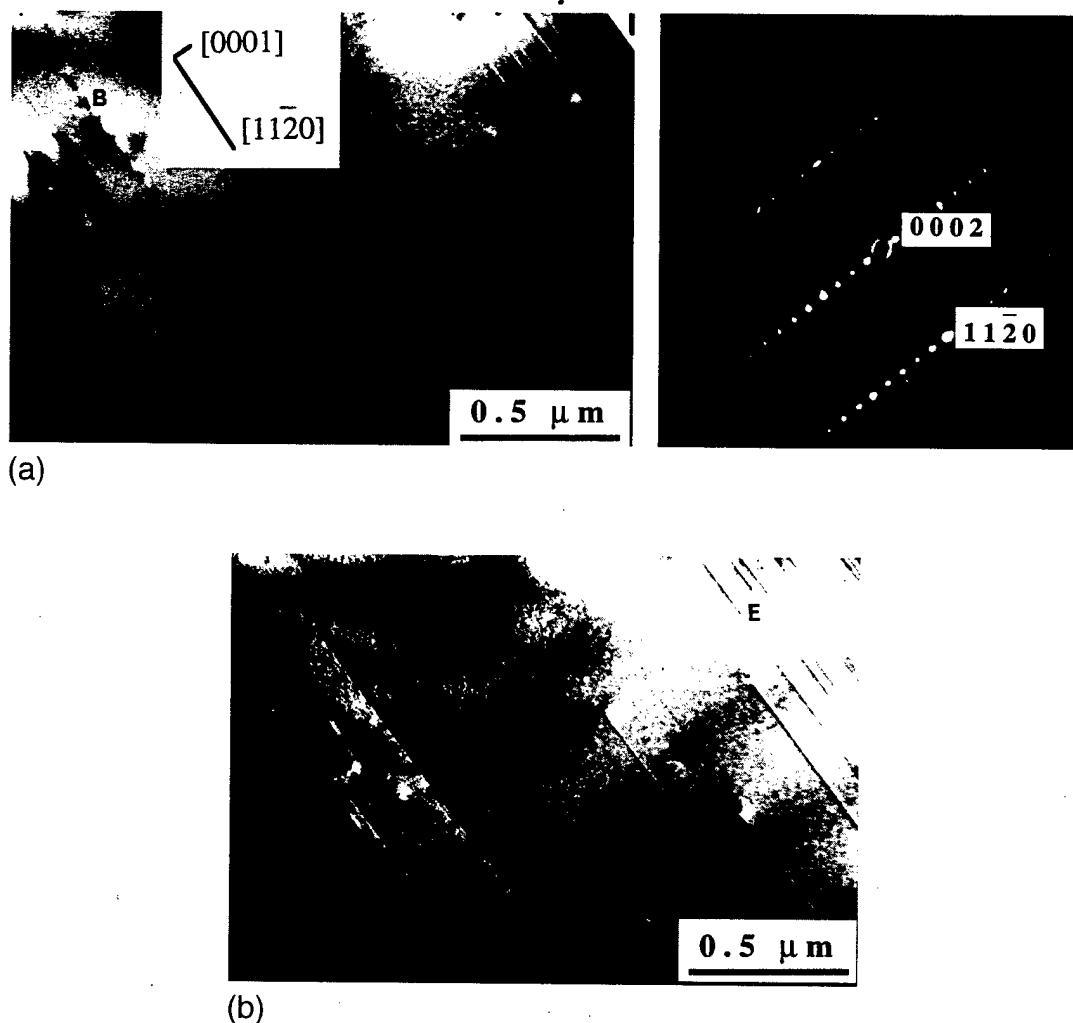


Fig. 3. Micrographs and corresponding selected area diffraction (SAD) pattern for a grain in an edge-on position: (a) bright field (nearest 0002 reflections were used in addition to the transmitted spot for this image); (b) centered dark tilt with  $11\bar{2}0$  reflection; B—dislocation array; (C) partials bounding stacking fault; (E) set of surface steps.

#### IV. Discussion

The most important result of this study is that basal plane dislocations are mobile and multiply as a result of room-temperature deformation. Direct evidence of dislocation mobility and multiplication in  $\text{Ti}_3\text{SiC}_2$  as a result of deformation



Fig. 4. Typical TEM micrograph after deformation at room temperature. Number and spatial extent of dislocation arrays is greatly increased compared to the undeformed samples.

can be seen in Fig. 4. The dislocation density is significantly higher after deformation than before (e.g., compare Fig. 4 with Fig. 1(a)). And while there are superficial similarities between the arrays shown in both cases, on closer inspection, they differ significantly. First, the number of these arrays in the undeformed samples is quite limited; Fig. 1(a) is more typical than Fig. 1(b). In the undeformed samples, the only dislocation arrays observed are adjacent to grain boundaries or cracks; the interiors of the grains are, for the most part, dislocation free. As a result of deformation, the number of arrays is greatly increased. Second, in the undeformed samples, the arrays only extend part of the way into the grain interior, typically 2–3  $\mu\text{m}$ . After deformation, however, the arrays extend across the whole field of view transparent in the TEM and thus, presumably, extend across the whole grain. It is worth noting that the grains are of the order of 3  $\mu\text{m}$  (the micrograph shown in Fig. 4 is that of a single macrograin) and thus the extent of these arrays is considerable.

A comparison of the TEM micrographs of the undeformed and deformed samples leaves little doubt that basal plane dislocations move and multiply at room temperature. This is in accord with the fact that  $\text{Ti}_3\text{SiC}_2$  plastically deforms at room temperature along the basal planes.<sup>5</sup> Furthermore, the absence of slip systems other than basal explains the brittleness of randomly oriented polycrystalline samples. Finally, the absence of cross-slip and dislocation entanglements explains the ease and extent by which  $\text{Ti}_3\text{SiC}_2$  forms kink bands<sup>5</sup> when the basal planes are parallel to the load direction.

Given what is currently known about the structure of  $\text{Ti}_3\text{SiC}_2$ , the fact that the defects are confined to the basal planes is not surprising.  $\text{Ti}_3\text{SiC}_2$  is a layered hexagonal material in which almost close-packed planes of Ti are separated from each other by hexagonal-nets of Si; every fourth layer is a Si layer. A basal interatomic vector is the shortest full translation vector in this structure; consequently perfect dislocations should have a Burgers vector of  $\mathbf{b} = \frac{1}{3}\langle 1\bar{2}10 \rangle$  and lie in the basal planes as observed. Other dislocations are much less likely because their Burgers vector would be quite large. The  $(0001)[11\bar{2}0]$  slip system is common to all hexagonal metals as well.<sup>11</sup> It is thus not too surprising that perfect basal plane dislocations with Burgers vector  $\frac{1}{3}\langle 11\bar{2}0 \rangle$  exist in  $\text{Ti}_3\text{SiC}_2$ . Nevertheless, this is the first report detailing the Burgers vector of dislocations in  $\text{Ti}_3\text{SiC}_2$ .

As a result of the long processing anneal at 1600°C, it is assumed that any dislocations formed as a result of plastic flow in the hot-press anneal out, an assumption that is consistent with the low defect density observed. The arrays of perfect basal dislocations (B in Fig. 1(a)) most likely form during cooling as a result of thermal residual stresses resulting from the anisotropy in the thermal expansion coefficients along the *c* and *a* axes. These dislocations appear to be emitted from the grain boundaries at triple junctions.

Concerning the stacking faults observed, errors in stacking sequence can occur during synthesis, or alternatively, can be formed as the result of the dissociation of a perfect dislocation into two partials. In the latter case the resulting stacking fault would be bounded by these partials. The most likely dissociation reaction is

$$\frac{1}{3}\langle 11\bar{2}0 \rangle \rightarrow \frac{1}{3}\langle 10\bar{1}0 \rangle + \text{SF} + \frac{1}{3}\langle 01\bar{1}0 \rangle$$

Since the perfect dislocation and the two partials have their Burgers vector lying in the same basal plane, it follows that the stacking fault bounded by these partials must also lie in that plane. These partials, in turn, can move conservatively in the basal plane and contribute to the deformation process. Such partials can be formed by dissociation of dislocations lying in

the grain boundaries in such a way that only the formed partial would be able to move conservatively. In that case, stacking faults would be limited from one side by grain boundaries as indeed was observed in this study (Figs. 1(b) and 2(c)). The stacking faults and the core structure of dislocations are now being investigated by analytical and high-resolution TEM, and the results will be reported in the near future.

## V. Summary

Deformed and undeformed samples of  $\text{Ti}_3\text{SiC}_2$  fabricated by the reactive hot pressing of Ti, SiC, and graphite was characterized by TEM. The undeformed material was single phase, and characterized by a low defect density. The vast majority of the dislocations and stacking faults observed were found to lie in the basal planes. The basal plane dislocations move and multiply as a result of room-temperature deformation. No evidence of dislocation entanglements or cross-slip was observed after deformation.

## References

- <sup>1</sup>M. W. Barsoum and T. El-Raghy, "Synthesis and Characterization of a Remarkable Ceramic:  $\text{Ti}_3\text{SiC}_2$ ," *J. Am. Ceram. Soc.*, **79** [7] 1953–56 (1996).
- <sup>2</sup>M. W. Barsoum and T. El-Raghy, "A Progress Report on  $\text{Ti}_3\text{SiC}_2$ ,  $\text{Ti}_3\text{GeC}_2$  and the H-Phases,  $\text{M}_2\text{BX}$ ," *J. Mater. Synth. Proc.*, **5**, 203–22 (1997).
- <sup>3</sup>M. W. Barsoum, T. El-Raghy, and L. Ogbuji, "Oxidation of  $\text{Ti}_3\text{SiC}_2$  in Air," *J. Electrochem. Soc.*, **144**, 2508–16 (1997).
- <sup>4</sup>T. El-Raghy, A. Zavaliangos, M. W. Barsoum, and S. Kalidindi, "Damage Mechanisms Around Hardness Indentations in  $\text{Ti}_3\text{SiC}_2$ ," *J. Am. Ceram. Soc.*, **80**, 513 (1997).
- <sup>5</sup>M. W. Barsoum and T. El-Raghy, "Room Temperature Ductile Carbides," submitted for publication in *Metall. Trans.*
- <sup>6</sup>S. Arunajatesan and A. H. Carim, "Symmetry and Crystal Structure of  $\text{Ti}_3\text{SiC}_2$ ," *Mater. Lett.*, **20**, 319 (1994).
- <sup>7</sup>J. Morgiel, J. Lis, and R. Pampuch, "Microstructure of  $\text{Ti}_3\text{SiC}_2$  Based Ceramics," *Mater. Lett.*, **27**, 85–89 (1996).
- <sup>8</sup>T. Goto and T. Hirai, "Chemically Vapor Deposited  $\text{Ti}_3\text{SiC}_2$ ," *Mater. Res. Bull.*, **22**, 1195–208 (1987).
- <sup>9</sup>W. Jeitschko and H. Nowotny, "Die Kristallstruktur von  $\text{Ti}_3\text{SiC}_2$ —Ein Neuer Komplexcarbidge-Typ," *Monatsh. Chem.*, **98**, 329–37 (1967).
- <sup>10</sup>J. J. Nickl, K. K. Schweitzer, and P. Luxenberg, "Gasphasenabscheidung im Systeme Ti–C–Si," *J. Less Common Met.*, **26**, 283 (1972).
- <sup>11</sup>R. W. K. Honeycombe, *The Plastic Deformation of Metals*, Edward Arnold, London, U.K., 1984. □